2023

Evaluating the trade-offs of using additive manufacturing for liquid rocket engines

Joshua Buettner

EVALUATING THE TRADE-OFFS OF USING ADDITIVE MANUFACTURING FOR LIQUID ROCKET ENGINES

Joshua Buettner

A THESIS

Submitted in partial fulfillment of the requirements
for the degree of Master of Science in Aerospace Systems Engineering
in
The Department of Mechanical and Aerospace Engineering
to
The Graduate School
of
The University of Alabama in Huntsville
December 2023

Approved by:

Dr. L. Dale Thomas, Research Advisor
Dr. Robert Frederick, Committee Chair
Dr. Judith Schneider, Committee Member
Dr. Keith Hollingsworth, Department Chair
Dr. Shankar Mahalingam, College Dean
Dr. Jon Hakkila, Graduate Dean

Abstract

EVALUATING THE TRADE-OFFS OF USING ADDITIVE MANUFACTURING FOR LIQUID ROCKET ENGINES

Joshua Buettner

A thesis submitted in partial fulfillment of the requirements for the degree of Master of Science in Aerospace Systems Engineering

Mechanical and Aerospace Engineering

The University of Alabama in Huntsville
December 2023

Liquid rocket engines (LRE) are among the most expensive components of any launch vehicle. While additive manufacturing (AM) shows promise in alleviating some of the costs of LREs, the use of AM could introduce new failure modes which would increase time spent in Test-Fail-Fix. This thesis demonstrates a methodology for understanding the trade-offs of using additive manufacturing for LREs to inform decision making. A decision matrix was used to choose the ideal AM process, and a quantitative model was applied to capture one of the trade-offs of using AM, that being increased surface roughness on LRE performance. A candidate component was selected for this methodology, and an ideal AM process was chosen. The results showed there was minimal loss in performance due to increased surface roughness. Demonstrating this methodology showed how a model-based approach to systems engineering can help engineers make informed decisions before going to the test stand.

Acknowledgements

I would like to take a moment to acknowledge the people whose assistance made the writing of this thesis possible and therefore deserve special recognition. First, I would like to thank Dr. Dale Thomas for lending his wisdom to my efforts and providing guidance throughout this research process, both of which proved invaluable. Second, I would like to thank Dr. Robert Frederick, who has taught me much in the classroom and provided input and guidance on this work. Third, I would like to thank Dr. Judith Schneider for providing guidance as well as feedback on this work. Fourth, I would like to thank Marshal Space Flight Center Liquid Engine Office for sponsoring this work.

I would also like to thank Shreyas Lakshmipuram Raghu for his support and guidance in this work. Lastly, I would like to thank my family for their support and encouraging words.

Table of Contents

List of Figures

List of Tables

“Essentially, all models are wrong, but some are useful.”

– George E.P. Box

Chapter 1. Introduction

This chapter will introduce the background and context for the ideas presented in this thesis, including the motivation for this research, the research objective, and the thesis organization. The introduction will provide the necessary definitions and fundamentals to introduce the reader to RS-25 Affordability, Additive Manufacturing (AM), and Model Based Systems Engineering (MBSE).

1.1 Motivation

NASA's Space Launch System (SLS) plays a pivotal role in the upcoming Artemis missions, which plan to send manned missions back to the moon. SLS has the capability to send immense payloads to low earth orbit (LEO), which will prove vital to both Artemis and future NASA missions to Mars and beyond. Powering the core stage of SLS are two solid rocket boosters (SRB) and four RS-25 engines. Formerly known as the Space Shuttle Main Engine (SSME), the RS-25 engines are being reused for SLS, which will save NASA significant time and money to develop new engines [1]. Unlike the SSME era engines, however, the RS-25 will be expendable along with the rest of the SLS core stage. Given there are only 12 of these engines certified from the space shuttle era and NASA's future launch manifest demands Artemis missions through Artemis V, production restart for the RS-25 engine is required for missions beyond Artemis IV. Consequently, a production restart will require upgrades to the engine to interface with the new system. Also, given that RS-25 production closed down with the end of the Space Shuttle Program, a production

restart presents an opportunity to upgrade the manufacturing processes with new manufacturing techniques such as AM.

Metal AM, while a young manufacturing process, has seen tremendous growth and usage across multiple industries including the aerospace industry. The reasons for this include the reduction in lead time, a reduction of material waste, expansion of the supply chain, rapid Test-Fail-Fix (TFF) cycles, faster time to market, and lower buy-to-fly ratio [2]. Against subtractive manufacturing, AM utilizes a layer-by-layer fabrication method. The advent of AM techniques has reduced lead times to produce complex rocket propulsion components and decreased development costs drastically [3]. Within NASA, AM utilization for rocket engine components has been initiated and insights are being assessed from the Additive Manufacturing Demonstrator Engine (AMDE) [4,5]. With numerous hot-fire tests, these demonstrations showed that AM is a viable option for fabricating rocket engine components including injectors, combustion chambers, channel walled cooled nozzles, and augmented spark ignitors. During the SSME era, AM was not a proven concept; therefore, traditional techniques were used. Now that the SSME is the RS-25 engine, and engine production has to be restarted, some of components will be upgraded using AM. AM utilization for RS-25 components include augmented spark igniters, the nozzle (scaled to 65%), and a pogo accumulator [3–5]. As AM is at its infant stages of development, there exists an opportunity to bridge the technology challenges such as understanding material relationships and scalability in terms of structural, process, and performance relationships [5]. In this thesis, ten different AM processes shall be considered for the development of a decision framework utilizing a model-based approach [2] and [6]:

Table 1. AM processes and abbreviations [6].

AM Process	Abbreviation
Laser powder bed fusion	L-PBF
Electron beam powder bed fusion	LP-PBF
Laser powder direct energy deposition	LP-DED
Laser wire direct energy deposition	LW-DED
Arc wire direct energy deposition	AW-DED
Electron beam wire direct energy deposition	EBW-DED
Ultrasonic additive manufacturing	UAM
Additive friction stir deposition	AFS-D
Cold spray	CS
Binder Jet	Binder Jet

L-PBF and EB-PBF are the most commonly used in the aerospace industry, however, to make this research more comprehensive, all ten processes were considered. Given the diversity and nuances of each AM process, the art of selecting the appropriate process for a rocket engine component could prove daunting.

Lessons learned from past liquid rocket engine (LRE) developments indicate that a 75% of the development costs are spent on Test-Fail-Fix or TFF [7–9]. TFF is the process of uncovering and addressing failure modes within a system through rigorous testing. A reduction in TFF cycle cost would thus have a substantial impact on the programmatic costs of an LRE. Therefore, investigating the factors contributing to TFF cycle costs, such as time spent in the Fail-Fix portion of TFF, can have a significant impact on LRE programmatic costs [10].

While AM attributes may be beneficial in terms of optimizing TFF to almost any system, they are not universal. For instance, the reduced lead time of printing a part could vary greatly depending on the part and the AM process being used. Furthermore, minimum TFF cycles may be acceptable for an LRE, but for an advanced propulsion system such as

a Nuclear Thermal Propulsion (NTP) engine, there is a need to reduce the "Fail-Fix" portion of TFF. Therefore, an opportunity exists to develop a decision framework with respect to AM utilization for design change instances in legacy engines such as an RS-25 engine. This becomes progressively more difficult as system complexity increases. To remedy this issue, MBSE tools provide the appropriate framework and traceability needed to ensure the system analyses trace back to requirements and fulfill the purpose of the system [11–15].

MBSE is a formalized application of modeling to various System Engineering (SE) based activities such as system requirements, design, analysis, verification, and validation spanning across the life-cycle phases of the system. In MBSE, models replace documents as the primary artifact of the SE processes [16]. For rocket engine development, MBSE has helped automate verification and validation (V&V), maintain traceability, and shorten times for post-processing test data [11]. MBSE has also been beneficial to NASA's Design for Reliability (DFR) and Model Based Mission Assurance Activities (MBMA) [12–15]. To maintain traceability, assess the benefits, and perform trades of AM for a rocket engine development scenario over its lifecycle, it would be beneficial to pursue a model-based approach.

While it would be possible to perform independent analyses to evaluate the AM material relationships and scalability, it is also important to trace the lead time benefits to overall system performance, reliability, and test strategies leading to subsequent certification of the engine. MBSE can help view these benefits by leveraging a model-based framework.

1.2 Research Objective

The objective of this thesis is to develop a methodology which will inform decisions regarding AM for LRE using the RS-25 in an affordability context. Due to the number of criteria to consider when evaluating a parts suitability for AM, a decision methodology will be used to evaluate all the criteria for each of the AM processes. However, qualitative measures will only provide high level insight and more quantitative models are required to capture the general trends of using AM for LRE components. This is done through a first principles analysis which assesses the effects of surface roughness from additively manufactured parts on engine performance. This will also provide insight into how MBSE can be utilized to manage analyses and traceability in complex systems while also informing AM strategies for RS-25 affordability (to understand material relationships and scalability). Consequently, this thesis will demonstrate how MBSE can be utilized to formulate better test strategies and decrease the time in the TFF cycle.

1.3 Thesis Organization

This chapter introduced the fundamental ideas and background needed to understand the motivation for this research, that being developing methods to assess AM for LRE for the purpose of affordability. The focus of this thesis will be assessing the trade-offs of using AM for LRE's using RS-25 as a design example. Chapter 2 will delve deeper into the background of the RS-25, AM's applicability to LREs, MBSE, and trade studies. Chapter 2 will also establish the specific research questions being investigated in this thesis.

Chapter 3 will detail the methodology used to answer the research question developed in Chapter 2. The methodology is split into two sections, one will be the qualitative analysis, and the other will be the quantitative analysis. Chapter 4 will present the results as well as a discussion of the results. Chapter 5 will conclude this thesis with a final discussion of the results and how they apply to the research questions established in Chapter 2. Chapter 5 will then conclude with suggestions for future work which could build off of this research.

Chapter 2. Literature Review

As introduced in Chapter 1, factors contributing to TFF cycle costs, such as time spent in the Fail-Fix portion of TFF, can have a significant impact on LRE programmatic costs [10]. As briefly mentioned in Chapter 1, AM has the potential to provide cost benefits as well as potentially increase reliability by decreasing the number of parts. However, the performance trade-offs of using AM need to be understood in order to make informed decisions regarding test planning and manufacturability. For instance, if a part is created using AM and the cost and lead time on the part are reduced, but the part underperforms on the test stand thus increasing time spent in TFF, the added programmatic costs could exceed the cost savings of using AM. Therefore, the lead time to recertification must be significantly reduced to ensure the cost savings from AM produce a positive return on investment. This necessitates trade studies to help engineers make these informed choices regarding the use of AM for rocket engine components. If the trade space is not well defined, or the bounds of the trade not understood, this can lead to the omission of important data and uninformed decisions later in development. Consequently, the goal of this thesis is to demonstrate a methodology to build and evaluate the trade space to make informed decisions on AM utilization for RS-25 upgrades. This methodology, in turn, will allow for progress to be made toward RS-25 affordability by decreasing the time spent in the Fail-Fix portion of TFF.

2.1 RS-25

The RS-25 engine is an efficient and reliable rocket engine due to its extensive flight history during the space shuttle era when it was known as SSME. Formally known as the Space Shuttle Main Engine (SSME), the RS-25 is the core stage main engine for NASA's Space Launch System (SLS). With a sea level specific impulse of 366 seconds and a sea level thrust of approximately 1,859,264 N (418,000 lbf) at 109 % power level [17], the RS-25 boasts high efficiency and performance, enabling SLS to transport large payloads to Low Earth Orbit (LEO) and beyond [18–20]. After the space shuttle era came to an end, 16 certified SSME's remained. Now after the launch of Artemis 1 only 12 RS-25 engines remain. NASA now has enough engines, assuming no failures, for Artemis Missions through Artemis IV, necessitating a production restart. While the existing inventory of SSME's are being upgraded for immediate SLS missions, production restarts demand rigorous cost reduction objectives to be met for the major engine components [21]. To meet the cost reduction objectives, design changes to the engine are inevitable. Due to the expendable nature of the SLS-core stage it is necessary to make the RS-25 engines more affordable to adapt them to that use. While the Space Shuttle flew with a three-engine configuration and reused its main engines, the SLS is configured to fly with four expendable engines [21]. Accommodating the configuration change also demands design upgrades to the existing engines, which require recertification via TFF. The need for TFF increases the development costs significantly, decreasing the affordability of the engines. Recently, Aerojet Rocketdyne began testing a redesigned RS-25 for Artemis V and beyond [22], yet TFF still needs to be optimized.

2.2 RS-25 Affordability

Delivering affordability for rocket engine development utilizing MBSE is a part of a progressing research effort. The affordability framework was envisioned and developed in [23] combining an RS-25 engine model and a gray box model of SLS which includes a first principles payload performance model and a breakdown of SLS configurations. The RS-25 engine model was constructed to capture the steady state performance of the engine which would allow for sensitivity analyses to be performed. The crucial advantage of integrating the models into an affordability framework is that trade factors are now linked across interfaces in the system rather than at the interfaces. Therefore, any change at the component level can be assessed in reference to the overall system and not just component level Technical Performance Measures (TPMs).

The launch scrubs of Artemis I also reiterate the need to develop approaches that can overcome the inherently high costs of TFF. Launch scrubs add to the programmatic costs of the Artemis program, and having the ability to foresee the reasons for these scrubs could eliminate future scrubs for the program. For instance, the first two launch attempts for Artemis I were scrubbed on August 29 and September 3 due to a hydrogen leak in an interface between the liquid hydrogen fuel feed line and SLS [24]. Interface issues such as these can be foreseen early in the development lifecycle if the interface is captured properly in a model-based realm.

The affordability framework utilizes the Systems Modeling Language (*SysML*) to leverage MBSE. *SysML* is a graphical modeling language that provides the semantics to perform various SE activities such as requirement analyses, behavioral analyses, performance and needs analyses, and simulation [16]. The structural aspects of the model

can be expressed using block definition diagrams (*bdd*) and internal block diagrams (*ibd*). The behavioral aspects can be represented using use-case diagrams (*ucd*), activity diagrams (*act*), state machine diagrams (*stm*), and sequence diagrams (*sd*). The requirements can be represented using a requirement diagram (*req*), the model organization can be modeled using package diagrams (*pkg*), and the mathematical formulations can be represented using parametric diagrams (*par*) [25]. All of these diagrams are tools within SysML which aid in the modeling process, meaning they are not all required to model a system successfully or effectively. For example, the functional behavioral aspects of RS-25 affordability framework are modeled using the *ucd* and *act*.

Figure 1 provides a visual representation of the affordability framework which consists of four aspects to deliver affordability: Structural Models, System Component and Performance Models, Functional and Behavioral Models, and Other Engineering Analysis Models.

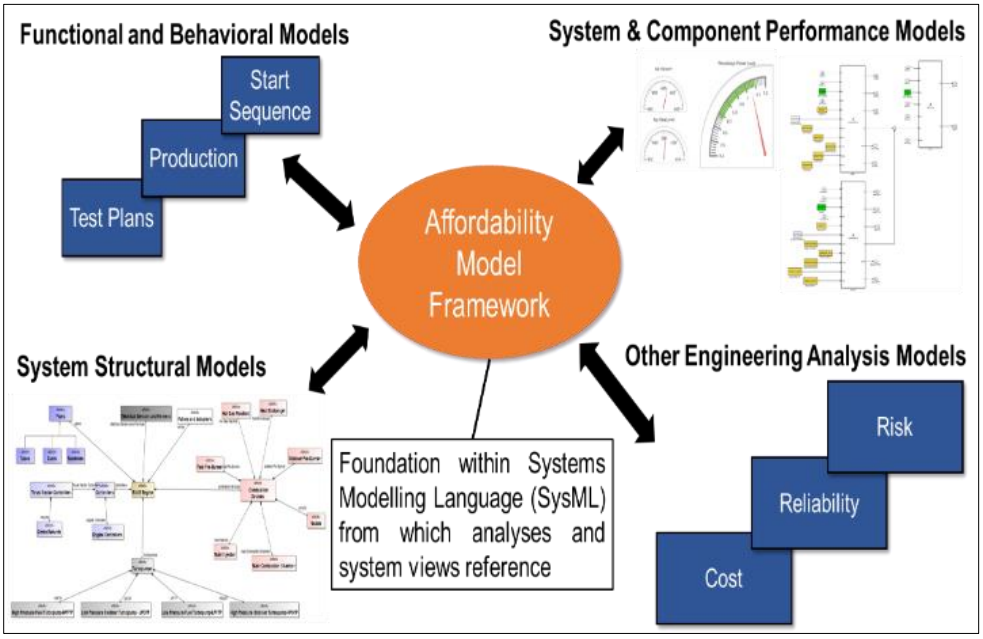

Figure 1. The Affordability Modeling Framework for the RS-25 [23,25–27].

Once the framework was established and the structural and performance models were developed in [23], the functional and behavioral models were initiated in [25]. By modeling RS-25 behavioral elements (performance, test strategies, design change implementation) in a digital realm, the influence of design change scenarios is captured earlier in the system lifecycle. Subsequently, the trade-offs can be weighed allowing for informed decisions early in the lifecycle of the engine [25].

The primary behavioral model for RS-25 was developed in [25] and is comprised of use-cases and actors. These use-cases present a functionality in terms of how a system is used by external entities to accomplish a set of goals or success scenarios, and the actors represent the entities which act on the system [16]. The development of use-cases needs to be relevant to significant aspects that drive the affordability for the RS-25 production restart, therefore the primary use-case which initializes the RS-25 Affordability *ucd* is the *Restart Engine Production* use-case. This research is being jointly pursued by NASA's Marshall Space Flight Center (MSFC) in Huntsville, Alabama and the Complex Systems and Integration Laboratory (CSIL) at the University of Alabama in Huntsville (UAH); therefore, two actors are used to represent how the RS-25 Affordability Framework is being developed on a programmatic level.

The primary behavioral model as a *ucd* for a rocket engine production is expressed in Figure 2 [25]. While the *ucd* is expressed for an RS-25 engine context, the utility is generic in nature to be applicable to multiple rocket engine architectures.

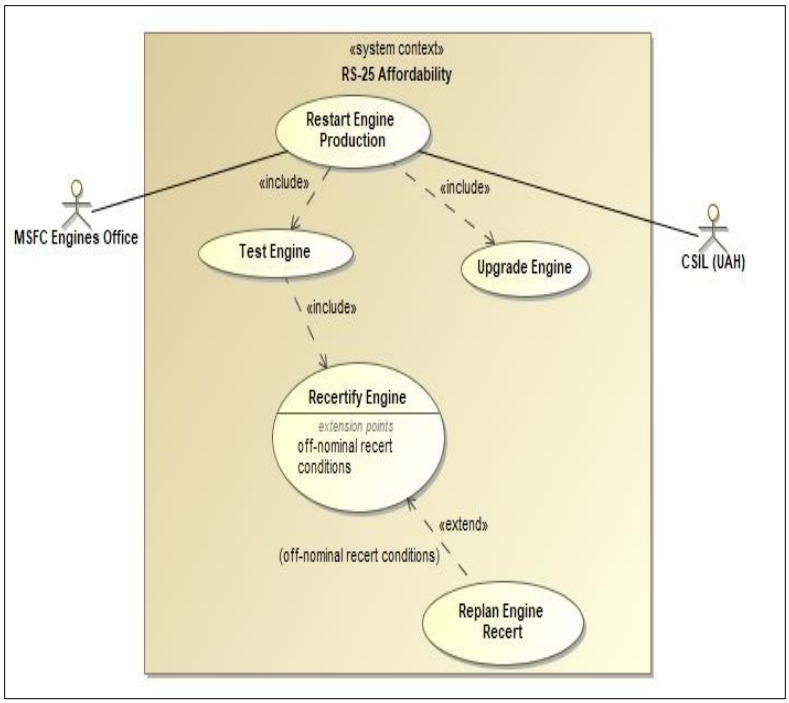

Figure 2. The primary use-case diagram (*ucd*) for RS-25 Affordability [25].

The main success scenario of the *Restart Engine Production* use-case is to analyze the impact of a design change to the RS-25 engine and assess of the number of tests and reliability utilizing the modeling environment (affordability model framework) leading to successful production and recertification of the RS-25 engine [25]. To achieve this success scenario, the *Restart Engine Production* use-case includes two other use-cases, *Test Engine*, and *Recertify Engine*. These use-cases were refined to smaller use-cases and actionable sequences represented as *act* in [25], and [27] which cover part of the success scenario for the *Restart Engine Production*, specifically development of test strategies and reliability.

To fully achieve the success scenario for the *Restart Engine Production* use-case, the actionable aspects of the *Upgrade Engine* use-case must be developed to analyze the impact of a design change. Therefore, the scope of this thesis is within the behavioral

modeling framework for the *Upgrade Engine* use-case and description as seen in Figure 3 and Table 2, as well as the other engineering analysis models referring back to Figure 1.

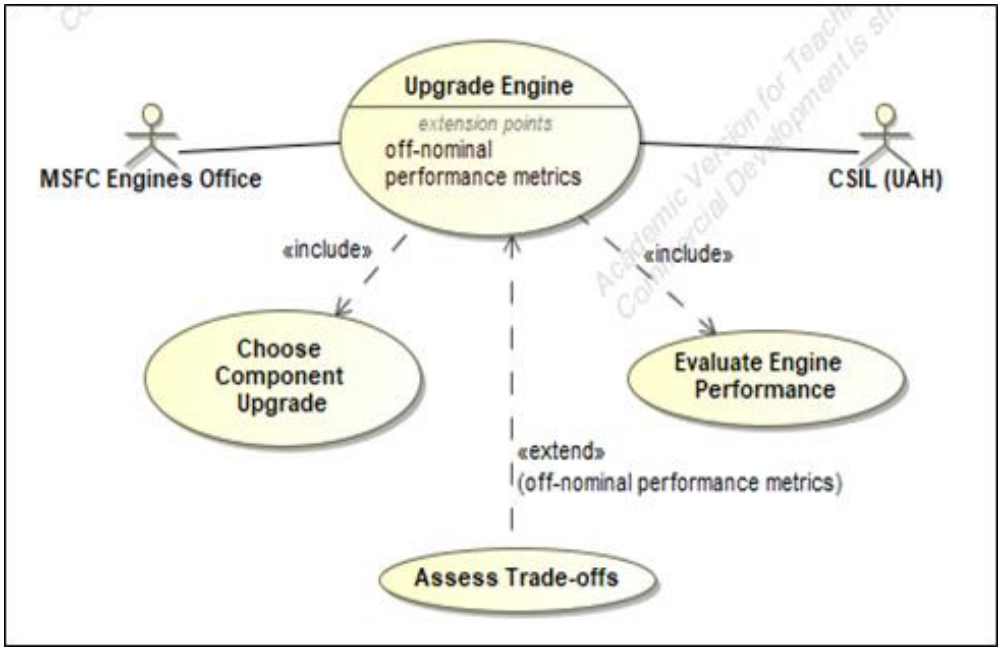

Figure 3. The *Upgrade Engine* use-case [25].

Table 2. Description of *Upgrade Engine* use-case [25].

Use-Case: Upgrade Engine **Scope:** The RS-25 engine affordability platform shall be developed in a modeling environment to reduce time spent in Test-Fail-Fix cycle for future production restart, test and recertification of the engine. **Primary Actor (s):** MSFC Engines Office, CSIL (UAH) **Secondary Actor (s):** Program Manager (MSFC), Principal Investigator (CSIL, UAH) **Stakeholders (s):** NASA, UAH **Pre-conditions:** Information of RS-25/SSME engine architecture (SSME era) and lessons learned, and candidature of an RS-25 engine component with major cost-reduction objective. **Post-conditions:** A successful component upgrade yielding nominal engine performance for the engine with trade-off's due to component upgrade analysed. **Trigger:** A major component of an RS-25 engine (SSME era) requiring design upgrade **Main Success Scenario:** The component of the RS-25 engine is chosen for a design upgrade, the performance and trade-offs are analysed with respect to the upgrade situation utilizing the modeling environment (affordability model framework) leading to successful production and recertification of the RS-25 engine. **Extension Points:** off-nominal performance metrics

It can be seen from the descriptions in Table 2 that the primary use-cases are driven by the fundamental objective of shortening the time spent in TFF cycle and decreasing lead time for recertification of the engine. Therefore, the modeled use-cases describe the high-level capabilities that holds significant relevance to the factors contributing to the TFF cycle: redesign and remanufacturing (*Evaluate Engine Performance*, and *Choose Component Upgrade*), retest (*Test Engine*), and recertification (*Recertify Engine*). These *ucd*'s demonstrate a systematic way to view of the capabilities that are necessary to achieve the objective [25].

In summary, the research study on the envisioned affordability model aspects include:

- The development of system component and performance models are demonstrated in [23].
- Structural Models based on cost reduction objectives developed in [25].
- For Other Engineering Analysis Models, initiation of a Model Based Failure Modes, Effects, and Criticality Analysis (FMECA) is demonstrated in [26].
- The Functional and Behavioral Models have been developed concurrently with other affordability aspects in [23,25–27].

Initial work investigating AM for RS-25 using MBSE [26,27] sought to link reliability requirements to AM effects. Due to the evolving nature of AM literature on failure and its characterization, it is difficult to extrapolate AM effects on the overall system. Therefore, it is beneficial to develop a comprehensive SE methodology to simplify the AM decision making process. Methods to simulate the mechanical and metallurgical effects of AM were investigated to potentially help predict the reliability of AM components. One method was developed by Rodgers *et al.* [28] which creates 3D synthetic

microstructures over large regions using an idealized molten zone and temperature-dependent grain boundary mobility implemented in a Monte Carlo model. While this model shows promise, there are concerns with augmenting this method to suit the needs of a model-based affordability context as presented in this study due to limitations in the model. For example, the simulation domain fixes geometry and therefore does not recreate residual stresses, temperature-induced slumping, or collapses of overhangs. Also, the model does not consider temperature accumulation over the entire course of the build, which is significant when considering powder based AM processes [28].

2.3 Additive Manufacturing for Rocket Propulsion

The AM processes listed in Table 1 are classified based on the state of the material (melted or not melted), the heat source, and the feedstock type (powder, wire, foil, or barstock), feedstock referring to the form the metal takes before entering the machine/process [6]:

- L-PBF fabricates parts by melting the shape of the part one layer at a time into a bed of metal powder. Once each layer is done, a re-coater spreads another layer of powder, and the laser begins sintering the next layer. Once the part is done, the excess powder is removed, and the part is removed from the build plate.
- EB-PBF is similar to L-PBF but differs in that it uses an electron beam to melt the powder inside a vacuum chamber.
- Direct Energy Deposition (DED) processes are characterized by the use of a robotic system to move the deposition head and the material is melted at the same time that it is being deposited. The types of DED processes are as follows:

    - LP-DED, as the name suggests, uses a laser to melt powder in the shape of each part layer.
    - AW-DED uses an electric arc to melt a wire feedstock.
    - LW-DED uses a laser to melt a wire feedstock.
    - EBW-DED uses an electron beam as its heat source and a wire feedstock to feed material into the build.

The most diverse set of AM processes require no melting of the material and are therefore categorized as solid state and are as follows:

- UAM induces metallurgical bonding between thin layers of foil by using a high frequency transducer at approximately 20,000 Hz and constant high pressure.
- AFS-D is unique in that it uses powder or solid feedstock. It deposits the feedstock into a friction stir pin tool and applies downward force to induce plastic deformation and deposit the feedstock in a layer-by-layer fashion.
- Cold Spray uses a supersonic converging diverging nozzle to inject high pressure inert gas and metal powder against a surface to form the part.
- Binder jetting extrudes metal powder feedstock infused with a binding agent into the part shape. The part is then cured in a chemical bath which removes the binder agent, then it is sintered in a furnace.

Both technical and programmatic criteria must be considered to adequately evaluate the AM processes. Gradl *et al*. [6], after extensive work on process selection criteria for AM, distills the list of criteria to eight primary parameters: 1) Industrial Maturity, 2) Part Complexity, 3) Feature Resolution, 4) Scale of the Part, 5) Required Properties and Material Physics, 6) Speed of the Process (closely related to cost), 7) Availability of the

Process and Supply Chain, and 8) Integrated Materials using Bimetallic or Monolithic alloys. Industrial Maturity refers to the technological maturity of each process. While AM has been around for decades, most AM processes are not the same age or at the same level of maturity. For example, L-PBF was one of the first metal AM processes and therefore has had more extensive testing. This technological maturity level can be captured using Technical Readiness Level (TRL) [29]. There also exists other methods for capturing process maturity such as Manufacturing Readiness Level and Integration Readiness Level [30], however TRL is the most commonly used in the aerospace industry particularly at NASA. *Part Complexity* refers to how well a process handles highly complex parts with intricate designs and internal lattice structures. *Feature Resolution* defines how small of a feature on a part the printer can manage and is dependent on layer thickness, feedstock size, and heat source diameter. *Scale of the Part* refers to the dimensional requirements for the printer to print the required part. *Required Properties and Material Physics* is largely dependent on what the part is intended to do. For example, if the part being assessed is structural, the mechanical properties of that part are most important, and by that token the mechanical properties produced should be compared when making the decision. These properties could also include physical ones such as thermal conductivity or pressure drop (due to surface roughness). *Speed of Process* refers to the speed at which the printer can fabricate a part and is directly linked to the deposition rate. *Availability of the Process and Supply Chain* refers to the number of vendors producing machines for that specific process and availability of the feedstock. *Integrated Materials using Bimetallic or Monolithic alloys* refer to the ability of the process to handle multiple alloys at once when printing a part.

To illustrate the potential benefits of AM, the cost and lead time of a printed 156 kN thrust Bimetallic Combustion Chamber was compared to the same part manufactured traditionally by Gradl *et al*. in [2]. The results indicate a schedule reduction of 56% on the initial AM process, and a reduction of 72% after the AM process was improved. In terms of cost, the initial and the improved AM processes saw a reduction of 35% and 60% respectively. Another benefit of AM is the ability to print highly complex parts and internal structures that would otherwise be impossible utilizing conventional manufacturing techniques [2].

While AM provides many benefits, these must be weighed against the potential detriments to avoid a net negative effect. The benefits of AM will vary depending on the process used, the machine, the part being printed, and the context in which the part is being fabricated. The mechanical properties of AM parts are often a subject of investigation. For instance, some AM processes produce parts with higher porosity and higher surface roughness than traditionally manufactured parts [6]. Consequently, the nature of qualification and verification of parts made by AM is a matter of concern since existing non-destructive evaluation (NDE) capabilities are not optimized for AM processes [31]. Though AM can in theory print highly complex parts, the higher complexity may only be achievable with lower deposition rates and more post processing which potentially decreases the lead time to produce the part. Furthermore, supply chain factors will often constrict the usage of AM as well. For example, a certain component may require a specific material, but a shortage of the feedstock of that material which the machine requires results in a supply chain concern.

While some of these concerns can be addressed through certain post processing techniques or by lowering the deposition rate, this may offset the lead time gains originally obtained by printing the part. Consequently, in this study the surface roughness effects of each AM process on the RS-25 engine Large Throat Main Combustion Chamber (LT-MCC) will be assessed. Note that not all these AM processes are suitable for LT-MCC fabrication due to scalability, Technical Readiness Level (TRL), or materials optimized for each process. The purpose of this study, however, is to perform a comprehensive study of all AM methods. By including all AM methods, future work can investigate areas of improvement for AM processes currently not suitable for this component.

Considering high speed flows in rocket engine components such as the LT-MCC, Turbopumps, Channels, Ducts etc. are common, surface roughness of the interiors of these components becomes a tremendous concern. With an increase in surface roughness, there are two major effects. The first effect, which will be the focus of this study, is an increase in skin friction and a pressure loss across a flow path due to this friction. Second, which will be the focus of a future study, is an increase in heat transfer due to increased surface area. While a rocket nozzle would seem like an obvious candidate for a study of these effects, the RS-25 nozzle geometry is outside of the capabilities of most of the AM processes and will be the focus of future work. Consequently, the analysis in this paper focuses only on the hot gas side of the RS-25 LT-MCC without the nozzle extension.

While surface roughness is usually compensated for using post processing, this adds to the lead time of the part. To make matters more complicated, deposition rate is roughly correlated to part cost, and while higher deposition rate AM processes potentially produce cheaper parts, the increase in deposition rate results in higher surface roughness.

Therefore, deposition rate will not be investigated in this thesis. These trade-offs constitute the need for trade studies to be conducted to make the most effective decision regarding AM upgrades.

2.4 Trade Studies

Trade studies are an essential part of any engineering process as they provide a formal process for choosing between alternatives given a desired outcome. The primary objective of a trade study should be to make informed decisions when selecting the best alternative. This is done by forming a list of viable solutions, exploring the merits of each alternative relative to the criteria established in the trade space, assigning scores to each alternative based on their merits, and rank order the alternatives based on score [32]. In the case of RS-25 Affordability, trade studies are an essential part of the *upgrade engine* use-case as seen in Figure 3. While there are many ways to conduct a trade study, most follow a general pattern. Below is an example from [33]:

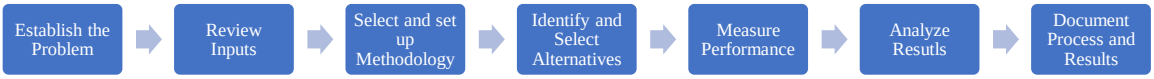

Figure 4. General Trade Study Process as presented by the Department of Defense in [33].

Wasson provides a more detailed example utilizing utility functions in [32]:

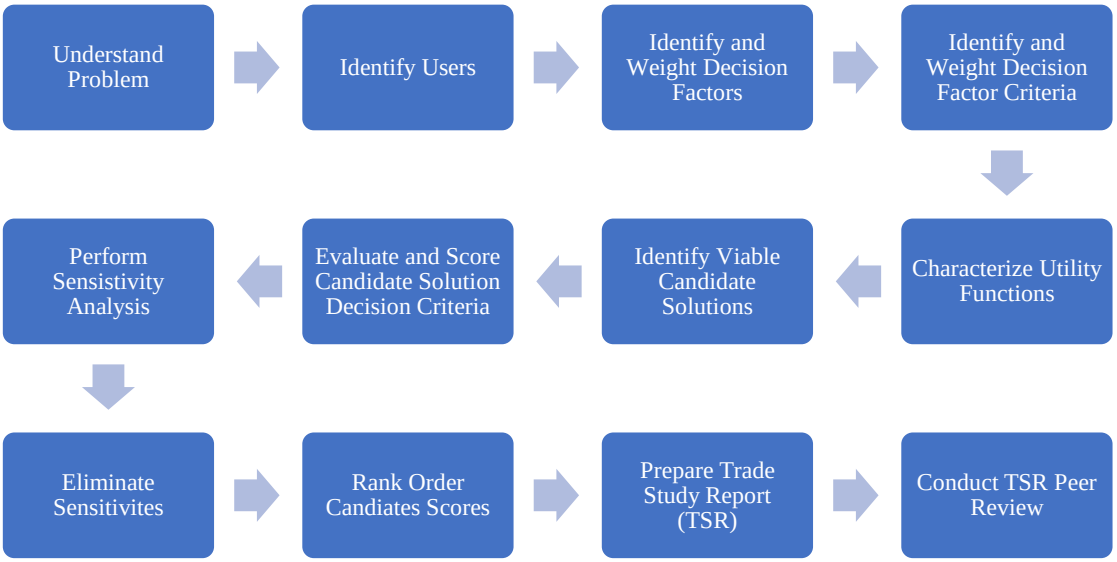

Figure 5. Wasson's trade study process [32].

In both examples, the trade study starts with the problem statement. In the case for RS-25, the problem being investigated can be captured using the question: What is the optimal AM solution for RS-25 which maximizes performance while minimizing lead time? A detailed and comprehensive trade study for the RS-25 is part of the ongoing affordability framework, and the research presented in this thesis focuses on measuring the performance of each of the viable AM candidates.

It is important to note; this research does not describe the entire trade study process, as creating a good trade study hinges on the involvement of the entire integrated team [33]. In a system engineer role, this includes input from subject matter experts, and the methodology developed for this research is set up in a way as to allow future input from other technical teams.

2.5 Summary of Literature Review

While the RS-25 engine is a high performing high reliability engine, production must be restarted in order to meet NASA's future launch demand for Artemis [21]. By far the highest development cost, historically, for the SSME era engines was the recertification process, traditionally done through TFF [23]. From the literature review it was found that AM offers lead time and cost benefits which were not available during the SSME era. Given the number of AM processes, however, choosing the ideal AM process for a select component requires evaluation of multiple criteria. In addition to this, the potential detriments of AM, specifically surface roughness, have to be understood and predictable in order to develop effective affordability strategies using AM.

This necessitates the following research questions:

Research Questions

How is LRE performance affected by AM, specifically surface roughness?

How can MBSE aid in LRE Affordability?

Chapter 3 of this thesis will outline the methodology for measuring performance and scoring/ranking the alternatives. First, the methodology will comprehensively and qualitatively assess the trade-offs of using AM based on Gradl's work. Next the methodology will present a physics based mathematical model quantifying one of the trade-offs of using AM, and while this model will focus on surface roughness on the hot-gas side of the LT-MCC, the physics, math, and framework can accommodate other trade-offs. What this methodology will provide is a baseline for making informed decisions regarding AM and RS-25 engine production and testing.

Chapter 3. Methodology

The goal of this methodology is to present a comprehensive analysis of AM processes being considered for an RS-25 component. It will provide a qualitative assessment of the criteria established in Chapter 2, it will perform a quantitative assessment of one of the trades needed to be made in an AM design change instance, and it will demonstrate how MBSE aids in the speed and accuracy of this process. In the systems engineer role, the goal is to develop models which capture general trends and behaviors. Once this is done, subject matter experts are consulted to refine the models and provide the predictability needed to support the affordability effort.

The choice of component for this methodology, as mentioned in Chapter 2, is the RS-25 Large Throat Main Combustion Chamber (LT-MCC). This choice was made based on the LT-MCC's high failure rate in the SSME era testing [34], as seen in Figure 6, and its high impact on the performance of the overall engine. Note that the information on the RS-25 used in this methodology is based on publicly available data on the SSME and RS-25 engines.

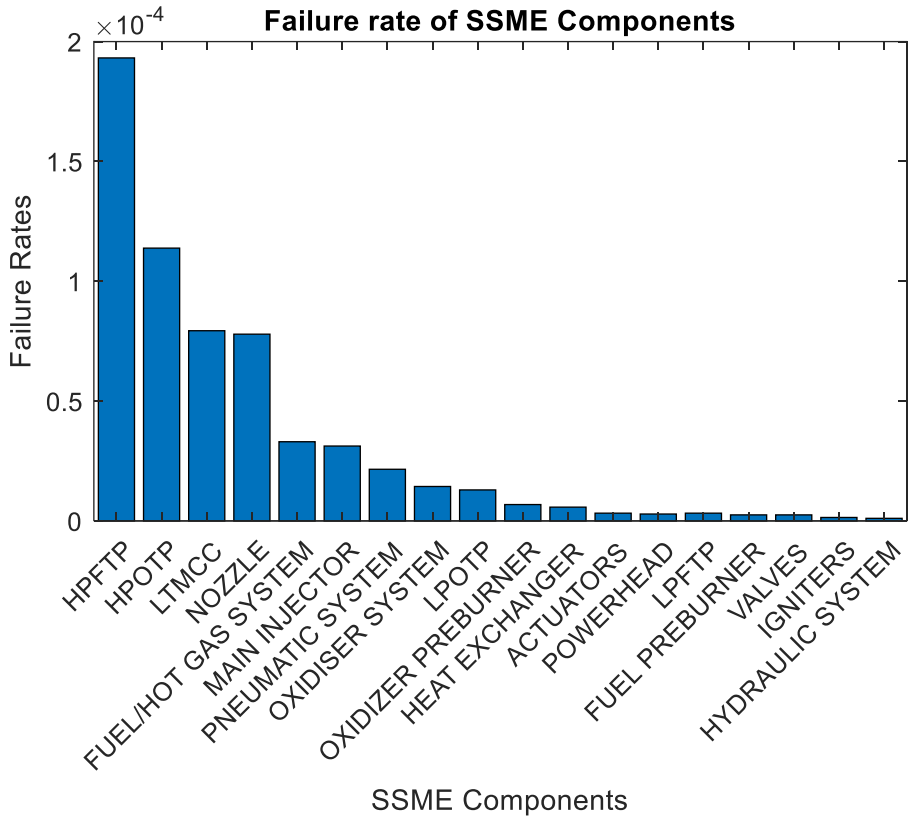

Figure 6. Reliability failure rates SSME components recreated based on [34].

3.1 Qualitative Model

As previously discussed in Chapter 2, use-cases provide a means to capture how a system is used by external entities to accomplish a set of goals [16]. The utility of capturing these use-cases in use-case diagrams was developed in [23,25–27] and summarized in Chapter 2. As the views for realizing the objective are established, it is important to model the actionable sequences that govern the realization of the established capabilities. Subsequently, this helps assess the required leads for the reduction in time for recertification of the RS-25 engine. In SysML, this can be achieved through activity diagrams (*act*) which model the behavior in terms of flow of inputs, outputs, and control [25]. As seen in Figure 7, the rounded rectangle in an *act* represents a call behavior action

required for accomplishment of the activity. The solid hollow circles represent the initial and termination points of the activity. The dashed (flow of action) and solid arrows (object flow) represent the transition between actions of the activity, and the solid horizontal and vertical lines represent concurrent behavior of actions. The diamond represents the decision points in the activity, and the squared-parentheses over a transition represents a condition necessary for the successful transition of flow [16].

The *Choose Component Upgrade* use-case, defined in Figure 3, is refined into an *act* expressing the actionable sequence, Figure 7. Similar to *ucd's*, the actions in a primary activity can be further refined to a set of actions in another activity diagram. This behavior is indicated on an activity through a rake symbol in an action of the activity as seen in Figure 7 [25].

As previously established in Chapter 2, AM is an attractive manufacturing alternative to traditional manufacturing methods especially for rocket engine components However, the potential benefits of AM have to be compared to the potential detriments in order to make informed decisions. Therefore, it can be seen that the modeled course of actions involves an assessment of feasibility for utilizing an AM technology for the production of a chosen component upgrade within the realm of availability of a 3D printing capability.

Given the ten AM options conferred in Chapter 2, the initial approach when deciding what AM option is best for a given part was to invest time into assessing all ten options. NASA's Systems Engineering Handbook states the purpose of NASA Pre-Phase A project life cycle phase is, "To produce a broad spectrum of ideas and alternatives for missions from which new programs/projects can be selected, and to determine the

feasibility of [the] desired system, develop mission concepts, draft system-level requirements, assess performance, cost, and schedule feasibility; identify potential technology needs, and scope" [35]. Limiting factors such as money, time, and workforce hinder this trade space exploration, however, and this same dilemma applies when trading between AM methods. Therefore, it is necessary to conduct this trade space exploration in an efficient manner, performing a top-down, boundary condition informed allocation of constraints-based approach to accessible trade space identification [36]. As shown in Chapter 2, both trade study approaches presented allow for this type of top-down approach. In the first example from the Department of Defense (DOD), the fourth step when conducting a trade study is to "Identify and Select Alternatives" which leaves room for selecting viable candidates for study [33]. In the second example conceived by Wasson, the sixth step is to "Identify Viable Candidate Solutions" which also allows for the boundary condition approach [32].

Subsequently, a method was conceived to filter the AM prospects. This method defines the boundary conditions of a candidate part and eliminates the prospects which don't meet a basic set of criteria which are required to print that candidate part. This process is similar to a "go/no go" decision, and the criteria chosen are based on AM process constraints and NASA requirements. After the prospects have been screened, the shortened list of prospects moves into the trade space. In this section the trade-offs of using different AM processes will be assessed qualitatively using a simple decision matrix. This will provide a comprehensive baseline to build a higher fidelity model on top of once input from subject matter experts is obtained.

3.1.2 The Screening Process

Before the process can begin, the underlining assumptions which define the trade space have to be established. These are as follows:

1. Technical readiness level will be utilized to assess the industrial maturity of each AM process due to its extensive use at NASA [29] rather than Manufacturing Readiness Level (MRL) [30].
2. All candidate parts are assumed to be monolithic, *i.e.*, not considering bimetallic capabilities, as this will add further complexity and given this process seeks to set up and demonstrate a methodology, this complexity was deemed unnecessary.
3. There is no variability between AM machines sold by different vendors. In reality an L-PBF machine sold by one vendor will have different build dimensions and performance than another L-PBF machine sold by another vendor. Given the vast number of AM vendors in the market today, this assumption is meant to simplify the analysis and falls within the scope of this thesis in capturing the general trends of AM's effect on performance.

The first step for the screening process is encapsulated in the Screen AM Options action. The *Screen AM Options* action is envisioned to screen AM processes based on the AM decision criteria that are easy to In this case, three hard requirements were distilled from the eight primary parameters stated in Chapter 2 and defined in [6] and are as follows:

Table 3. Screening Criteria definitions.

Screening Criteria	Definition
Technical Readiness Level (TRL)	Systematic metric/measurement system that supports assessments of the maturity of particular technology and the consistent comparison of maturity between different types of technology [29].
Scale of the Part	Maximum build dimensions (height and diameter)
Material availability	Materials optimized for each process

Consequently, the *Screen AM Options* action is refined into actionable sequences as expressed in Figure 8. This screening process assesses the maximum build dimensions, materials optimized for each process, and process TRLs for printing a given part. The objective of the *Screen AM Options* action is to determine potential AM processes that are possible for a given part. These hard requirements will be referred to as *screening criteria* in the subsequent sections of the paper. The *screening criteria* will allow, given a selected part, for certain AM processes to be screened out of consideration in the overall trade and help reduce the number of processes for trade assessments. By screening out the impossible processes, the trade space is simplified and the possibility of selecting an impossible process in error is eliminated.

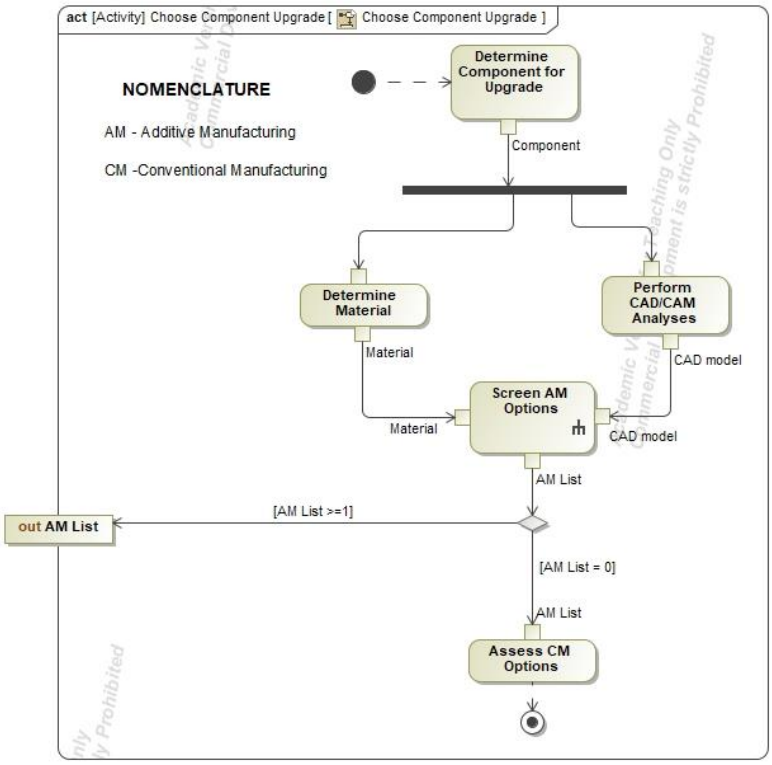

Figure 7. The Activity Diagram (*act*) for the *Choose Component Upgrade* use-case [37].

This process begins with an initial node and proceeds through a control flow to the first action *Assess Available Materials* that determines the optimized materials for each AM process as seen in Figure 8. This action requires an input called *Material* which is provided through an object flow and represents the material of the subject part. A comprehensive list of the most commonly used metals and alloys for different metal AM processes for propulsion applications is available in [2]. While the list is continually evolving, it provides an adequate starting point for screening out AM processes early in the decision-making process for the scope of this research. In this action, the list of all AM processes is screened based on what processes are optimized for each material. The output of this action is the new list of AM processes, called *AM List*, which is now shorter (in most cases) because the processes that are not optimized for the material of the chosen component are screened out.

The next action, called *Assess Dimension Requirements*, refers to the second screening criteria, and will input the AM List from the previous action. The *Assess Dimension Requirements* action relates to screening AM process based on their maximum build dimensions. This action compares the maximum build dimensions of each AM process to the part dimensions from the CAD model. The dimensions are input through an object flow from the activity parameter node *CAD model*. Much like the previous action, after the *AM List* is screened again, it is output through an object flow to the next action. For instance, if an arbitrary selected part has a dimension (height or diameter) that exceeds the limits of the maximum dimensions of the printer being evaluated, it is deemed impossible to print with that process and the process is screened out of consideration. The maximum build dimensions achievable by the ten AM processes are listed in Table 4.

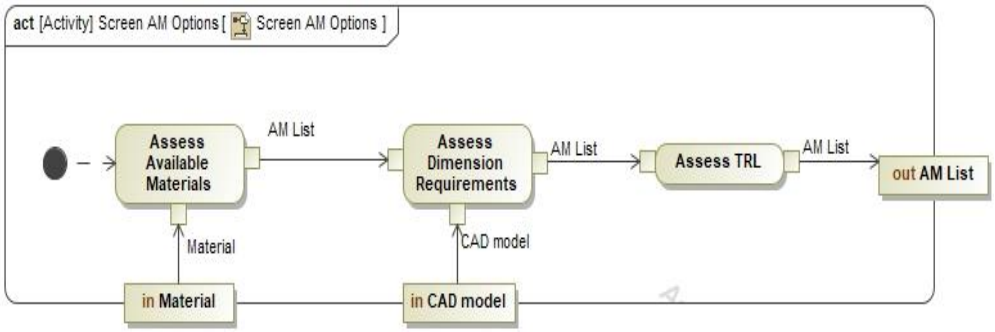

Figure 8. Refinement of the *Screen AM Options* action [37].

The maximum build dimensions were approximated from the information available in [2]. If the build dimensions were not available, it was synthesized from the build volume information available in [6].

Table 4. Typical max build dimensions for AM processes [37].

AM Process	Maximum Build Height (mm)	Maximum Build Diameter (mm)
L-PBF	1000	1000
EB-PBF	500	300
LP-DED	3700	3000
LW-DED	3750	2500
AW-DED	9000	5000
EBW-DED	3250	4000
UAM	1500	1800
AFS-D	1000	1000
CS	2750	4500
Binder Jet	464	464

The final action in the screening process is the *Assess TRL* action, which represents the final screening criteria. The *Assess TRL* screens the AM list based on a required TRL. This action inputs the AM list that has been screened for available materials and dimensional capability, compares the required TRL to the TRL of each AM process in the AM list, and eliminates the AM processes which do not meet the required TRL. The final AM list is then output with an object flow connected to the output activity parameter node called *AM List*.

For this study, the TRL of each process is obtained from [6] and [2]. The TRL limit can be set to whatever suits the needs of decision makers, but for this methodology a baseline TRL of 6 shall be chosen as it refers to the prototype demonstration in a relevant environment [29]. The ten AM processes and their TRLs based on required TRL of 6 are listed in Table 5. Given a component instance, an AM process with TRL less than 6 shall be screened out.

Table 5. TRL's for the AM Processes [37].

AM Process	TRL
L-PBF	≥ 6
EB-PBF	
LP-DED	
LW-DED	< 6
AW-DED	≥ 6
EBW-DED	
UAM	
AFS-D	< 6
CS	
Binder Jet	≥ 6

After the completion of this action, the final AM List can move along in the *Choose Component Upgrade* activity as seen in Figure 7. The screened AM options will then flow on to the assessment of trades encapsulated in the *Assess Trade-offs* use-case. If no AM processes are available for a given component instance, the conventional manufacturing method needs to be chosen, encompassed in the *Assess CM Options* action.

3.1.3 Assessment of Trades

The first method used to capture the trade-offs of using different AM processes is presented in this section. The more subjective criteria derived from the eight primary parameters detailed in Chapter 2 will be referred to as the *trade criteria*. These *trade criteria* are directly derived from the remaining five parameters established in Chapter 2 from [6]. The only deviation from these parameters is the exclusion of the last parameter, integrated materials using bimetallic or monolithic alloys. As previously established, one of the underlining assumptions of this study is that all the candidate parts will be monolithic.

The *trade criteria* and definitions for the screened AM options are as follows:

1.) *Part Complexity*: represents how well a process handles part complexity.

2.) *Feature Resolution*: represents how small of a feature the process can print (correlates with layer thickness)

3.) *Mechanical Properties and Physical Performance*: represents how well the part performs when manufactured with the process and is highly dependent on the intended function of the part.

4.) *Economics*: represents feedstock costs, machine build time, anticipated service life, and post-processing

5.) *Process Availability*: represents market availability of AM process with respect to process availability in-house, and if not the number of vendors that has the manufacturing capability to print the part.

Unlike the *screening criteria*, these represent the criteria that are harder to quantify to enable comparison with other AM processes. To illustrate, *Part Complexity* is critical when evaluating a printing process while the *Feature Resolution* requirement might offer flexibility based on the operating environment of the part. Subsequently, a decision maker may choose to forgo a certain AM process and trade resolution for another desirable trait while still maintaining the part's functionality. In this study, the *screening criteria* is meant to determine potential AM processes that are possible while the *trade criteria* are meant to choose the best process to realize the affordability potential for the component instance's development.

Decision making is an essential part of engineering, and assessing trade-offs can become difficult when faced with a staggering number of choices and criteria. This is only made more cumbersome when the criteria are difficult to quantify. There are several ways to assist the decision maker that are common practice in industry. One of the simpler methods is a decision matrix.

A decision matrix is formed by assigning weights to the *trade criteria* for a given component instance. The weights for each of the *trade criteria* are based on a simple scale, usually one to five. Next, each of the *trade criteria* are assigned a score for each candidate based on the information available in literature. The scores for each of the candidates are multiplied by the weights assigned to the respective candidate. Finally, a total score is obtained for each candidate by adding all the scores for that candidate together. The formulation for evaluating the total score is represented in Equation (3.1):

$$S_T = \sum_{n=1}^{m} w_n s_n \,, \tag{3.1}$$

where S_T represents the total AM process score, m is the total number of *trade criteria*, n is the *trade criteria* index, w represents the weight of the *trade criteria* assigned with respect to the component instance, and s represents the score assigned for each *trade criteria*.

When applied to the context of this research, the decision matrix shall also consider the Conventional Manufacturing (CM) option to trade the most viable AM process against the score of the conventional manufacturing technique. The weights for each *trade criteria* are based on a scale of 1-5 (5 being best and 1 being worst). Each of the ten AM methods, along with CM are assigned a weight based on the scale and definitions defined in Table 6

and are assigned based on engineering best judgment derived from literature [2,6]. The definitions of this scale with respect to each of the *trade criteria* are also listed in Table 6.

Table 6. Trade Criteria Scale [37].

Trade Criteria	Scale
Part Complexity	1 - Low Complexity, 5 - High Complexity
Feature Resolution	1 - Least Resolution, 5 - Highest Resolution
Mechanical Properties and Physical Performance	1 - Least Priority, 5 - Most Priority
Economics	1 - Least Economic, 5 - Most Economic
Process Availability	1 - Least Available, 5 - Most Available

The weights assigned to each of the *trade criteria* for the RS-25 component instance are shown below in Table 7.

Table 7. Weights for the RS-25 Component Instance [37].

Criteria Index (*n*)	Trade Criteria	Weights (*w*)
1	Part Complexity	2
2	Feature Resolution	2
3	Mechanical Properties and Physical Performance	4
4	Economics	4
5	Process Availability	3

Once the weights are assigned for each of the aforementioned *trade criteria,* each of the AM processes are assigned a score for each of the *trade criteria* based on the scale in Table 6. Each of these scores are then multiplied by the corresponding weight as defined in Table 7 to give the new score for each of the AM processes. The new scores for each process are then added to give a total score for each AM process

While this method offers a comprehensive look at the different criteria to consider when determining the best AM solution for a part, it is founded on a qualitative scale as seen in Table 6. While this method is also relatively easy and quick to implement, the qualitative nature of the weights and scores calls into question the objectivity of the results. To get a more accurate and objective reading on one of the trade-offs of using AM, one of the trade criteria will be evaluated in more depth, that being *Mechanical Properties and Physical Performance.* Section 3.2 will specifically focus on surface roughness and how it pertains to *Mechanical Properties and Physical Performance.*

3.2 Quantitative Analysis

While the previous section detailed a comprehensive methodology for making trades between AM processes, quantitative models need to be implemented to understand, in more detail, the trade-offs of using each AM process rather than relying on engineering best judgment. In reality, multiple analyses must be employed to consider all the attributes that go into assessing all trade-offs, however, for the purposes of demonstrating this methodology, the surface roughness trade-off will be the only one assessed. As mentioned in Chapter 2, there are many effects AM has on a part that could be detrimental to that part's performance. One of the known effects AM has on parts is increased surface roughness [2]. Higher surface roughness tends to correlate with build speed, defined in this context as deposition rate. While deposition rate gives an estimate of build speed [6], the increased surface roughness caused by the higher deposition rate will require more post processing and this will add to the overall lead time of the part and cost. In other words, one does not want to spend ten dollars in one area to save one dollar in another. Therefore, a better understanding of the effect increased surface roughness has on rocket engine

performance is needed to determine what margins of surface roughness an AM engineer can work with to deliver a part with minimized lead time and cost and maximized performance.

The scope of this research is limited to analyzing how surface roughness affects performance of an LRE. Focusing on surface roughness and its effect on performance, while not the only aspect of *Mechanical Properties and Physical Performance* for AM that should be analyzed, does provide insight into performance and, for the purposes of this thesis, provides a demonstration of the overall methodology with which other studies can be conducted. For instance, an analysis on fatigue life could be conducted utilizing this same framework, or an analysis of thermal conductivity would also fit well within this framework.

The surface roughness for this research is quantified as *Ra* or average roughness. This value is found by taking the arithmetic average of the distance from the average height of a profile [38]. The baseline values for surface roughness (*Ra*) for each of the AM processes, and the references they are derived from are listed in Table 8. The *Ra* for the AFS-D process could not be found from literature, the value however was estimated based on "extremely coarse" rating for the process in [6].

Table 8. AM processes and their respective surface roughness [39].

AM Process	*Ra* (*μm*)	Reference
L-PBF	5 - 10	[40]
EB-PBF	30 - 38	[40]
LP-DED	40	[41]
LW-DED	40 - 60	[42]
AW-DED	200	[42]
EBW-DED	200	[42]
UAM	7	[43]
AFS-D	250	[6]
CS	11.28	[3]
Binder Jet	15	[40]

To evaluate the overall effect of surface roughness on performance, the trade factors (in this case surface roughness) have to be linked across interfaces, as iterated in Chapter 2 [23]. It is therefore necessary to link the effects of *Ra* from an AM process to the performance elements of the engine [6]: specific impulse (I_{sp}) and thrust (F). The candidate component for this analysis will be the LT-MCC as gas pressure drops needed to flow the combustion products within the chamber should be a minimum; any pressure losses ahead of the nozzle inlet reduce the exhaust velocity and thus vehicle performance [44]. While this analysis will focus on surface roughness inside the chamber, these equations and approaches can theoretically be applied to any duct in the engine or other LREs. The same first principles approach and equations still apply to the main combustion chamber on any other LRE, granted the flow properties and geometry are updated to match the candidate component.

When modeling the physical behavior of a rocket component, tools such as Computational Fluid Dynamics (CFD) or Finite Element Analysis (FEA) are appealing for their physical accuracy and wide use across industry. However, high speed and high temperature flows are computationally expensive for a CFD code to solve with accuracy. If the number of alternatives can be reduced, the amount of time spent on alternatives which fall outside the margins will also be reduced making the trade study process more efficient [36]. It is therefore desirable to refine the trade space and reduce the number of prospects before employing such tools. Therefore, a simplified first principles approach was conceived for evaluating surface roughness effects on performance to capture the general trends of utilizing AM for LREs.

3.2.1 Geometrical and Flow Considerations

High speed flows in any duct are highly dependent on geometry and fluid properties [45]. Therefore, the geometry of the component has to be determined, but due to the fact that the scope of the RS-25 affordability framework established in Chapter 2 remains open source, the geometry of the component must be derived from public information. The geometrical and flow considerations are derived based on information available in the public domain for the LT-MCC geometry [46], for power level of 109% considering the Block II version of the engine. This version of the LT-MCC for SSME was recreated in CAD, Figure 9, using *SolidWorks* in order to, as accurately as possible, capture the geometry of the LT-MCC.

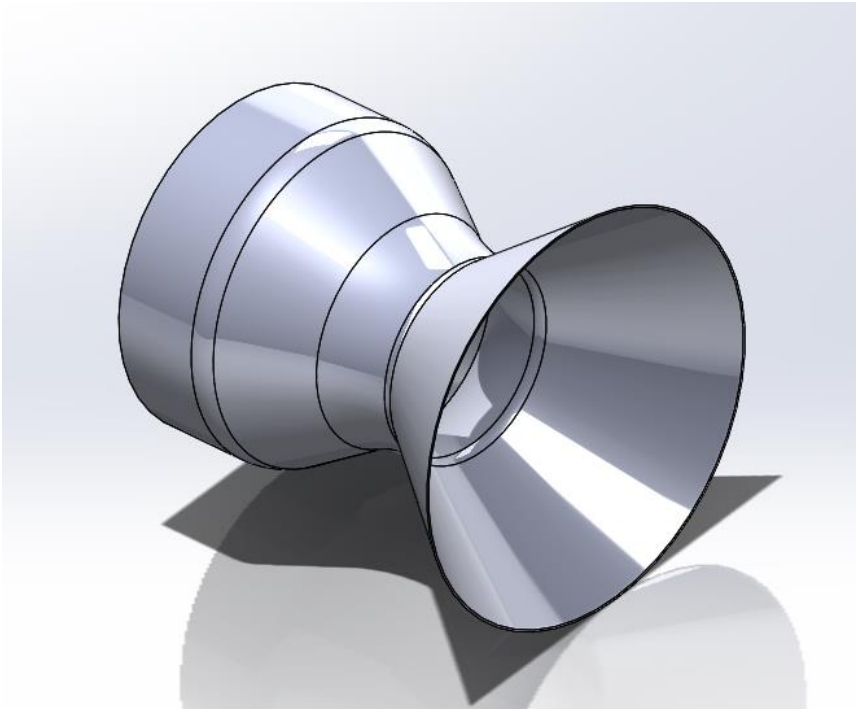

Figure 9. Isometric view of LT-MCC recreated using *SolidWorks*.

Consequently, a *MATLAB*® subroutine was developed to generate the cartesian coordinates for the LT-MCC geometry which is used in the subsequent equations to solve

for performance elements. The flow considerations in [46] are appropriately utilized to perform the performance analysis as detailed in Table 9.

Table 9. Estimated RS-25 parameters used throughout the analysis.

Constant parameters	Estimated RS-25 Values
Area of the throat (A_t)	0.0191 m^2
Area of the exit (A_2)	1.31 m^2
Expansion ratio (ε)	68.57
Earth gravity constant (g_o)	9.81 m/s^2
Specific heat ratio (k)	1.2
Mass flow rate ($\dot{m}$)	522.8 kg/s
Molecular weight (MW)	13.6 kg/kg-mol
Chamber pressure (p_1)	20.65 MPa
Ambient pressure sea level (p_a)	0.101325 MPa
Hot gas Temperature (T_1)	3661.7 K

3.2.2 Evaluate Nominal Engine Performance

Before factoring in the losses evaluated using the methods explained previously, it is important to evaluate the nominal performance based on isentropic flow relations [44,47]. The assumptions to determine the nominal performance come from [47] include:

1. Ideal homogenous gas
2. Adiabatic
3. Incompressible flow
4. Frictionless/negligible boundary layer (initially)
5. No shocks/discontinuities
6. Steady and constant flow
7. Axial and uniform flow
8. Frozen chemical equilibrium conditions

Once the nominal performance values are calculated, this methodology will attempt to reintegrate friction into the equation and eliminate frictionless/negligible boundary layer assumption.

First, chamber conditions, chamber temperature and pressure (T_1, p_1 respectively), nozzle exit and throat area (A_2 and A_t respectively), are obtained from SSME literature [46] as seen in Table 9. Next, the exit pressure, p_2, can be numerically calculated using Equation (3.2):

$$\frac{A_t}{A_2} = \left(\frac{k+1}{2}\right)^{\frac{1}{k-1}} \left(\frac{p_2}{p_1}\right)^{\frac{1}{k}} \sqrt{\frac{k+1}{k-1}\left[1 - \left(\frac{p_2}{p_1}\right)^{\frac{k-1}{k}}\right]}. \tag{3.2}$$

With exit pressure, the exit velocity, u_2, of the rocket engine can be calculated using Equation (3.3):

$$u_2 = \sqrt{\frac{2k}{k-1}\frac{R_u}{MW}T_1\left[1 - \left(\frac{p_2}{p_1}\right)^{\frac{k-1}{k}}\right]}, \tag{3.3}$$

where R_u is the universal gas constant. Once the exit velocity is calculated, the thrust (F) of the rocket engine is calculated using Equation (3.4):

$$F = \dot{m}u_2 + A_2(p_2 - p_3) . \tag{3.4}$$

Finally, specific impulse (I_{sp}) is calculated using Equation (3.5):

$$I_{sp} = \frac{F}{\dot{m}g_o} . \tag{3.5}$$

Once the nominal performance values are evaluated, the losses evaluated by Method 1, Method 2, and Method 3 are implemented to evaluate performance as follows:

3.2.3 Evaluation of Pressure Losses Due to Surface Roughness (Ra)

Obtaining pressure loss across a varying geometry such as an RS-25 LT-MCC is an interesting challenge. In a constant area duct, the pressure loss is easily obtainable. However, once cross-section area varies as seen in Figure 10 and flow conditions reach supersonic conditions and there is no direct analytical solution. One way to remedy this is by numerical integration. In other words, this method splits the geometry into small incremental segments with constant area, calculating the pressure drop for each segment and summing them to get the total pressure loss.

To calculate the varying geometry across the chamber, six functions for radius were derived in terms of length across the chamber. These equations were fit based on geometric data points measured in CAD. These functions were combined into a single piece-wise function shown in Equation (3.6):

$$r(x)=\begin{cases} r_{injector} & 0\le x<L_1 \\ r_1\sqrt{1-\left(\frac{x-5.222}{r_1}\right)^2}+6.737 & L_1\le x<L_2 \\ -0.5882934166x+12.92307289 & L_2\le x<L_3 \\ -r_2\sqrt{1-\left(\frac{5.222-x}{r_2}\right)^2}+14.9057 & L_3\le x<L_4 \\ -r_3\sqrt{1-\left(\frac{x-15.222}{r_3}\right)^2}+6.530 & L_4\le x<L_5 \\ 0.6995195368x-5.445329549 & L_5\le x<L_6 \end{cases}, \tag{3.6}$$

where the lengths, L_1 through L_6 are presented in Figure 10 which outlines the basic geometry of the RS-25 LT-MCC derived from SSME data from [46]. With this function for varying radius, r, the cross-sectional area at each point along the length of the LT-MCC can be calculated and converted to metric units.

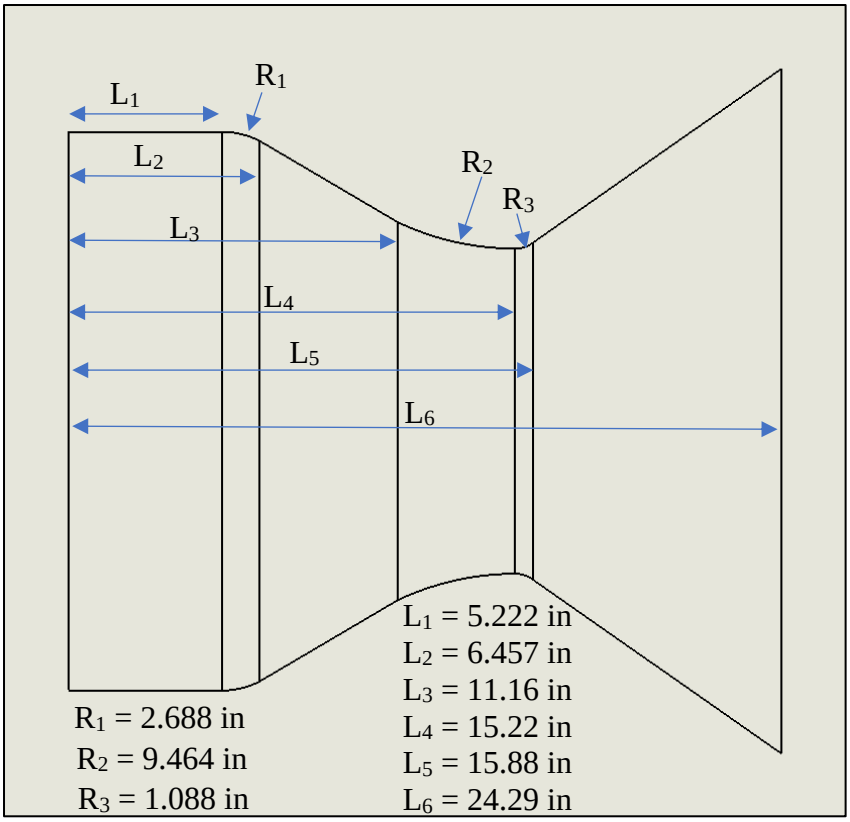

Figure 10. LT-MCC side view with relevant dimensions.

The power required to overcome the pressure loss (or head loss) can then be evaluated and used to determine the loss in kinetic energy (KE) of the rocket engine. With a loss in KE, the rocket propellant will have less exit velocity and subsequently lower performance for the engine. A second method was considered which takes the pressure loss as a direct loss of pressure in the chamber. Finally, a third method to find the pressure loss due to skin friction is through Fanno flow relationships rather than traditional isentropic flow relations. This however would restrict the geometry to the constant area section of the LT-MCC, as Fanno flow is simplified for a constant area geometry. All three of these approaches are based on first principles, and all three will be pursued in the preceding sections. The reason for developing all three methods is to compare the results of all three, and if all three show similar trends it will promote statistical significance of the general

trend of performance with respect to surface roughness. Note that all three methods are derived from first principles therefore making them universal to all LRE systems.

3.2.4 Method 1 (Energy Loss)

For this method, Darcy Friction Factor (f_D) must be calculated. This is done by calculating the Reynolds number (Re) using Equation (3.8) and numerically solving for f_D in Equation (3.7):

$$\frac{1}{\sqrt{f_D}} = -2\log\left(\frac{\varepsilon}{3.7D} + \frac{2.51}{Re\sqrt{f_D}}\right) \tag{3.7}$$

and

$$Re = \frac{\rho u D}{\mu}, \tag{3.8}$$

where ρ is the fluid density, u is the fluid velocity, D is the diameter, μ is the dynamic viscosity, and ε is the relative roughness calculated using Equation (3.9) [38]:

$$\varepsilon = 11.03Ra\,. \tag{3.9}$$

The LT-MCC geometry is segmented into small constant area segments each with a length of 0.1 inches. The head loss (h_L) of each segment is subsequently calculated using Equation (3.10):

$$h_L = \frac{Lf_D u^2}{2Dg_o}. \tag{3.10}$$

The total head loss and for the LT-MCC geometry is calculated using Equation (3.11):

$$h_{L_{total}} = \sum_{i=0}^{L} h_{Li}\,. \tag{3.11}$$

The next step in this method is to implement this head loss into the nominal performance equations. This method rederives the exit velocity equation based on first law

of thermodynamics accounting for the work done by the fluid to overcome the head loss (Method 1) in the LT-MCC. It starts with the first law of thermodynamics in terms of specific enthalpy as seen in Equation (3.12):

$$dh + vdv = dq - dw\,, \tag{3.12}$$

where *dh* is the change in enthalpy, *vdv* is the KE, *dq* is the heat flux, and *dw* is the shaft work done by the gases. With the adiabatic assumption, the *dq* term is negligible, and normally, when calculating exit velocity, the *dw* is also assumed to be negligible. However, since this analysis is accounting for increased skin friction, the work term will be left in. Following the same derivation of the exit velocity Equation (3.3) as in [47] but leaving in the work term gives Equation (3.13):

$$u_2 = \sqrt{-2\int dw + \frac{2k}{k\text{-}1}\frac{R_u}{MW}T_1\left[1- \left(\frac{p_2}{p_1}\right)^{\frac{k-1}{k}}\right]}\,. \tag{3.13}$$

This work term can be written as the power needed to overcome the head loss from the skin friction and must be divided by $\dot{m}$ since the Equation (3.13) is on a mass basis. The power to overcome the pressure loss can be obtained with Equation (3.14) [48]:

$$Power = h_{Ltotal}\dot{m}g_o\,. \tag{3.14}$$

Substituting Equation (3.14) into Equation (3.13) yields the new equation for exit velocity as expressed in Equation (3.15):

$$u_2 = \sqrt{-2\frac{Power}{\dot{m}} + \frac{2k}{k\text{-}1}\frac{R_u}{MW}T_1\left[1- \left(\frac{p_2}{p_1}\right)^{\frac{k-1}{k}}\right]}\,. \tag{3.15}$$

With the new exit velocity, the performance values are recalculated using Equation (3.4) and Equation (3.5).

3.2.5 Method 2 (Direct Pressure Loss)

This method follows a similar procedure to the previous method save for the last step and the integration into the performance model. For this method, Darcy Friction Factor (f_D) must be calculated. This is done by calculating the Reynolds number (*Re*) using Equation (3.8) and numerically solving for f_D in Equation (3.7).

The LT-MCC geometry is segmented into small constant area segments each with a length of 0.1 inches. The pressure loss (Δp) at each segment are subsequently calculated using Equation (3.16):

$$\Delta p = \frac{\rho L f_D u^2}{2D}, \tag{3.16}$$

The total head loss and pressure loss for the LT-MCC geometry is calculated using Equation (3.17):

$$\Delta p_{\mathrm{L}_{total}} = \sum_{\mathrm{i}=0}^{\mathrm{L}} \Delta p_{Li}\,. \tag{3.17}$$

The pressure loss calculated is directly subtracted from the chamber pressure and recalculating mass flow rate, exit velocity, and exit pressure. The pressure loss from skin friction ($\Delta p_{\mathrm{L}_{total}}$) obtained in Equation (3.17) is directly subtracted from the chamber pressure (p_1) as seen in Equation (3.18):

$$p_{1\_real} = p_1 - \Delta p_{L_{total}}\,. \tag{3.18}$$

With this new chamber pressure (p_{1_real}), the mass flow rate ($\dot{m}$) is recalculated using Equation (3.19) [44]:

$$\dot{m} = A_t p_{1\_real} k \frac{\sqrt{\left(\frac{2}{k+1}\right)^{\frac{k+1}{k-1}}}}{\sqrt{kRT_1}}. \tag{3.19}$$

With the new mass flow rate and p_{1_real}, the new Thrust (F) and I_{sp} can be calculated using Equations (3.2) - (3.5).

3.2.6 Method 3 (Fanno Flow Pressure Loss)

In this method, the pressure loss was calculated for the constant area section of the LT-MCC which is around 5.22 inches beginning at the inlet using the Fanno flow relations wrapped in the Aerospace Toolbox in *MATLAB*® [49]. While it is possible to account the varying geometric consideration (complete geometry) to Fanno flow relations, it is beyond the scope of demonstration in this study and warrants further research. The *MATLAB*® script used to implement this method is detailed in the appendix.

In this method, the chamber pressure (p_{1_real}) is recalculated based on Equation (3.18), but the $\Delta p_{L_{total}}$ is calculated from the Fanno Flow toolbox in *MATLAB*® for the constant area sections (until L = 5.222 inches). For this method, since it is only considering a small section of the combustion chamber, mass flow is constant (unlike in Method 2). With this new p_{1_real} for fanno flow method, F and I_{sp} are recalculated using Equations (3.2) - (3.5) as in Method 2.

3.3 MBSE Implementation

As seen in the previous section, one analysis done with three different methods is complicated. In a complex system, there is a multitude of components and analyses, and potentially hundreds of requirements that must be satisfied during analysis. One of the great

benefits to MBSE is the ability to trace requirements to analysis outputs. This makes system verification much easier during the development lifecycle of the system so when one component is changed the effects of that change are transparent and well understood across the rest of system where relevant. As opposed to document-based systems engineering, MBSE offers a faster more robust way to perform systems engineering tasks. Part of the objective of this thesis is to demonstrate how this is possible with one analysis example, and utility of pushing systems engineering into a model-based realm.

3.3.1 Analysis in Parametric Diagrams

As established in Chapter 2, *par* allow for mathematical formulations within SysML by capturing equations and functions with constraint blocks and modeling how they interact [16]. This enables system analyses to be performed within the model using values already established within the model. Typically, *SysML* tools allow for equations to be defined within constraint blocks in the software and this works efficiently enough for simple equations but can also be mathematically limiting. Given the surface roughness analysis established in this chapter involves many equations and some numerical methods to solve, *MATLAB*® is better suited for performing the actual analysis. This could pose a problem for the model; however, *MATLAB*® functions/subroutines are easy to implement as constraint blocks in *SysML par*. Having these subroutines captured in *SysML* in this manner allows for a user to run the model simulation without opening *MATLAB*® and run the analysis in the context of the system defined in *SysML*.

For the analysis presented in Section 3.3 of this chapter, the three methods for measuring performance losses in the LT-MCC due to increased surface roughness are captured in *SysML* within parametric diagrams as seen in Figure 11. Three subroutines

were created in *MATLAB*® and incorporated into the RS-25 affordability framework. See Appendix for the full *MATLAB*® subroutines. These subroutines are captured using constraint blocks with all the ports connecting the appropriate value properties inside the *Main Combustion Chamber (MCC)* block and connect to the value property outputs outside the blocks.

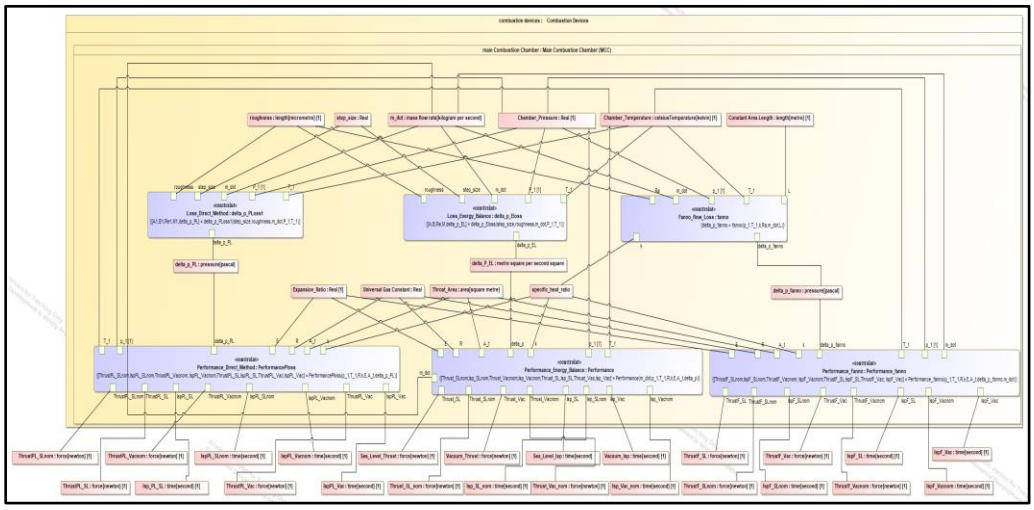

Figure 11. RS-25 engine surface roughness analysis parametric diagram in *SysML* [39].

The next step after running the analysis is to move the system into qualification after a design change instance is created. In this example ten design instances of the *Main Combustion Chamber (MCC)* block are created, each with a different surface roughness value. The *Main Combustion Chamber (MCC)* and *RS-25 Engine* blocks value properties are connected to the appropriate requirements as seen in Figure 12.

3.3.2 Requirements

As mentioned in Chapter 2, system requirements are captured using a *req* which allows for the relationships between requirements and the system to be modeled in *SysML*. Requirements pertaining to a specific value property of the system can be linked using a *satisfy* relationship. As the name implies, these relationships indicate that the value property of the system will satisfy the requirement it is connected to. Modeling this

relationship has many uses, but the most advantageous for a system like the RS-25, which in this context is going through recertification, is the ability to automate Verification and Validation (V&V) of the system.

With the requirements represented as requirement blocks and connected to corresponding values properties, the model will flag any requirement violations in the instance table with a red colored cell. This way the requirements validation is automated in *SysML*. While this analysis example in may seem trivial to implement in *SysML*, extrapolating this example to the entire RS-25 and including all the analyses to properly assess the trade-offs of using AM, one can see how the system becomes so complex, a formalized digital tool to organize everything become imperative.

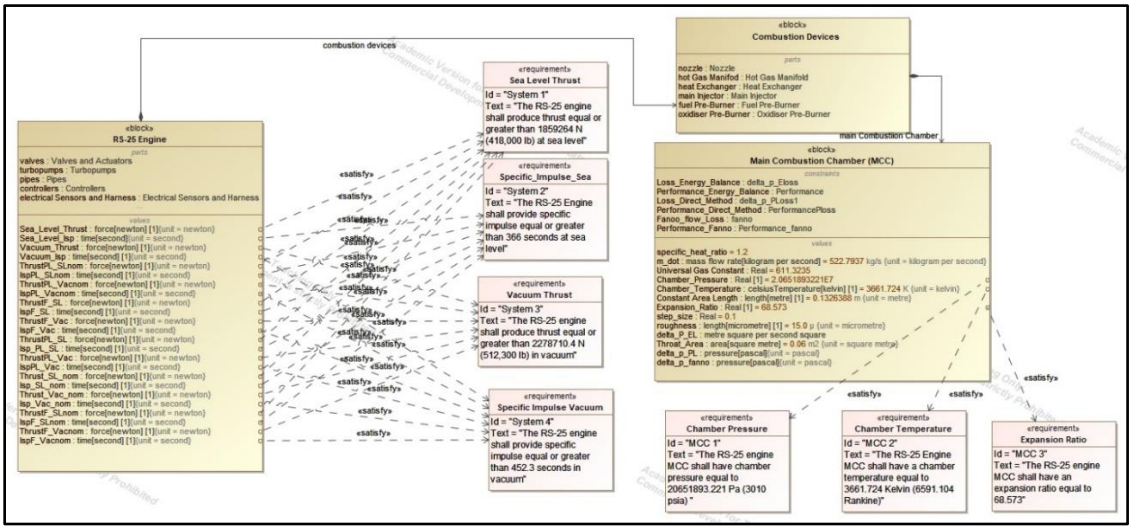

Figure 12. Requirement diagram (req) representing RS-25 engine and LT-MCC requirements and its association to the structural architecture [39].

3.3.3 Instance Tables

When conducting an analysis in a model-based realm, it becomes useful to conveniently store all of the instances of the model created during the analysis, especially when conducting trade studies. As seen in the example trade studies discussed in Chapter 2, Developing a TSR report and processing the results is a vital step in both trade study

examples. *SysML* allows for the creation of instance tables in which all the instances generated by a system analysis can be stored along with their respective properties (as specified by the user) [16].

After running the simulation, an instance table was set up to capture all the results for each of the ten design instances. Each time the simulation is run in *SysML*, ten instances of the LT-MCC are created and the analyses are run through the *MATLAB*® subroutines without having to open *MATLAB*®. These instance tables show the different AM processes used for each instance, the corresponding surface roughness values, the nominal performance values, and the new performance values accounting for losses. As shown in Figure 12, the corresponding requirements for RS-25 are linked to the value properties for each of the instances created by running the simulation. If one of the analysis output values is in violation of the requirement it corresponds to, that value/instance will be flagged (highlighted red). This simulation, therefore, automates the verification process of systems engineering. The instance table outputs for each of the methods used are presented in the appendix.

3.4 Summary

Chapter 3 presented a proposed methodology intended to answer the research questions established in Chapter 2. This methodology provides a way to quantify the criteria to consider when considering AM for LRE components. To help refine the trade space and provide more accuracy when assessing AM trade-offs, a model was developed which links surface roughness to LRE performance. Other models like this one can be employed to inform decisions regarding the use of AM for affordability. For example, as mentioned previously in this chapter, while this model focused on surface roughness in the

combustion chamber, another model analysis which focuses on structural fatigue life could be integrated into the process and factor into the *trade criteria*, *Mechanical Properties and Physical Performance*. The mathematics of a model like this would change, but implementation of the mathematics would remain intact. By adding analysis models to an already complex system, the use of MBSE to perform systems V&V and trace requirements becomes crucial. The next chapter will present the results of this methodology with the selected design case, the RS-25 LT-MCC. While this research was done in the context of RS-25 affordability, the methods are left generic enough as to accommodate other LRE and other propulsion systems.

Chapter 4. Results and Discussion

Chapter 2 showed how previous work sought to demonstrate methodologies to drive down the development cost for the rocket engine using RS-25 as a design example. Literature review indicates that while AM has many potential cost benefits, there are multiple decision criteria to consider when upgrading an engine component with AM. The lack of failure modes for AM parts and the number of AM processes make the implementation of AM while attempting to reduce engine failures a difficult task. This constitutes the use of trade studies in order to make the best decisions regarding the use of AM for rocket engines. Therefore, the research questions, restated here, were posed with the objective of informing decisions regarding the application of AM for LREs.

Research Questions

How is LRE performance affected by AM, specifically surface roughness?

How can MBSE aid in LRE Affordability?

The methodology presented in Chapter 3 sought to answer this question starting with a basic understanding of AM and past SSME data. As discussed in Chapter 3, the RS-25 will be used as a design example to demonstrate this methodology. A candidate part was selected, that being the LT-MCC based on the Block II data from SSME literature operating at a power level of 109%. Using the screening criteria detailed in Section 3.1, the AM processes not applicable were screened out to the trade space. One of the trade-offs of using AM for this component was then quantified regarding physical performance of the

component. A novel mathematical relationship between surface roughness and engine performance was established which can provide preliminary insight into the behavior of an upgraded component using AM, and act as a demonstration of how future analyses can be applied to this process.

4.1 Results from Qualitative Analysis

The approximate dimensions for the design change instance are summarized in Table 10. The diameter for the LT-MCC part is based on the structural jacket of the LT-MCC as is the maximum build height. For making a qualitative assessment of the LT-MCC, the structural jacket is approximated as a simple cylinder, as a highly detailed geometric model of the LT-MCC is unnecessary for a high-level analysis such as this. Therefore, the approximate cylinder shape was constructed and is visually depicted in Figure 13. Note here, that this cylindrical approximation cannot be made when conducting the quantitative analysis, due to the fact that, as mentioned in Chapter 3, the high-speed flows in the hot-gas side of the LT-MCC are dependent on geometry, therefore the geometry was preserved for that model.

As mentioned in Chapter 2 and Chapter 3, the material is Inconel 718 and is based on best available data from SSME era data [46]. Based on the *screening criteria*, the UAM process was eliminated due to material non-availability. The EB-PBF process was eliminated as the build dimensions of the LT-MCC are beyond the build dimensions

available for the process as seem in Table 4. AFS-D, CS, and LW-DED were eliminated as the required TRL baseline of 6 was not met as seen in Table 5.

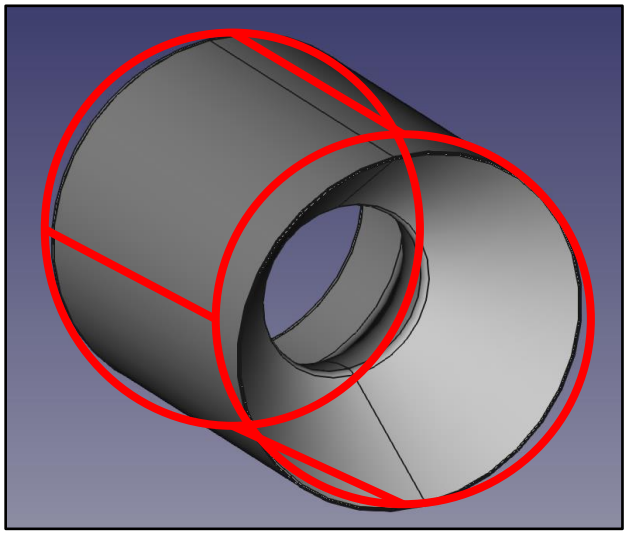

Figure 13. LT-MCC with approximate cylinder shape marked in red.

Table 10. Approximate dimensions of the structural jacket of the LT-MCC are used for the screening process.

Component	Material	Build Dimensions	
		Height (mm)	Diameter (mm)
Structural Jacket LT-MCC (RS-25 engine)	Inconel 718	373.4	450.6

The AM processes that flow into the trade space for *trade criteria* evaluations are L-PBF, LP-DED, AW-DED, EBW -DED, and Binder Jet. The weights (w) for the RS-25 LT-MCC are listed in Table 7. These weights were assigned based on the scale established in Table 6 from Chapter 3. *Part complexity* received a weight of 2 due to the low complexity and simple geometry of the structural jacket. *Feature resolution* also received a weight of 2 because the part selected has no small cavities or intricate patterns requiring high resolution. *Mechanical Properties and Physical performance* received a high weight of 4. This was due to the importance of mechanical and thermal properties for a rocket engine LT-MCC, as well as the desire to retain reliability in an RS-25 manufacturing

upgrade scenario. *Economics* received a 4 as well due to the importance of affordability in an RS-25 affordability context. Finally, *Process Availability* was weighted at a neutral 3, because while important, it is not more important than *Mechanical Properties and Physical Performance* or *Economics*.

Subsequent tables in this thesis will represent the *trade criteria* using their criteria index (*n*) as defined in Table 7. The scores (*s*) were assigned to the AM processes in the trade space and are listed in Table 11. The scores for these processes were assigned based on best available data regarding the current state-of-the-art technology for each AM process and conventional manufacturing (CM) that are comprehensively covered in [2] and [6].

Table 11. Scores for AM Processes and CM Process **[37]**.

n	**Scores (*s*)**					
	L-PBF	**LP-DED**	**AW-DED**	**EBW-DED**	**Binder Jet**	**CM**
1	5	4	3	2	5	3
2	4	3	2	2	4	4
3	4	4	2	2	3	5
4	2	3	5	3	3	1
5	5	4	2	1	4	4

Once the scores were assigned, the total scores (S_T) for the processes were obtained utilizing Equation (3.1) and are listed in Table 12.

Table 12. Final scores for AM Processes and CM Process **[37]**.

n	***w * s***					
	L-PBF	**LP-DED**	**AW-DED**	**EBW-DED**	**Binder Jet**	**CM**
1	10	6	6	4	10	6
2	8	6	4	4	8	8
3	16	16	8	8	12	20
4	8	12	20	12	12	4
5	15	12	6	6	12	12
S_T	**57**	**52**	**44**	**34**	**54**	**50**

The results indicate that the most viable AM process for the LT-MCC is L-PBF. It had the highest score of 57, followed by LP-DED and Binder Jet with scores of 54 and 52 respectively. The next process is Conventional Manufacturing (CM) with a score of 50, followed by AW-DED then lastly the EBW-DED. L-PBF scored highly in *Mechanical Properties and Physical Performance* and *Process Availability*, and while it scored lower in *Economics*, these were enough to propel it to the highest scoring process. AW-DED, while scoring highest in *Economics* (the highest score of any *trade criteria* interestingly), scored poorly in *Mechanical Properties and Physical Performance* as well as *Process Availability*. This result is a good illustration of the importance of considering all criteria (even lower weighted ones) when performing trades. A decision maker trying to pick a manufacturing process without this methodology may see the immense cost savings in AW-DED and decide to use it without considering its limited availability in the market or its lower performance, resulting in a suboptimal decision. The EBW-DED process had the lowest total score of 34 which indicates the need for improvements and further process developments to produce combustion chamber components for the scale of the RS-25 engine.

4.2 Results from Quantitative Analysis

The results of the *Ra* vs *Isp* and *F* (Thrust) are represented in Figure 14, Figure 15, and Figure 16. These plots were generated using a custom *MATLAB*® script and functions which are presented in the Appendix. After running the analysis in *SysML*, the results were verified against requirements. These graphs depict how the thrust and specific impulse change with respect to surface roughness. Thrust is colored red, Isp is colored blue, and the nominal performances are shown with dotted lines. The different AM processes are also shown on the graphs. As discussed in section 4.1, UAM, CS, EB-PBF, LW-DED, and AFS-D were all screened out in the screening process, therefore those processes are highlighted pink. The required thrust and specific impulses for sea level and vacuum conditions are also shown as text to give a reference to what the requirement is.

A. **B.**

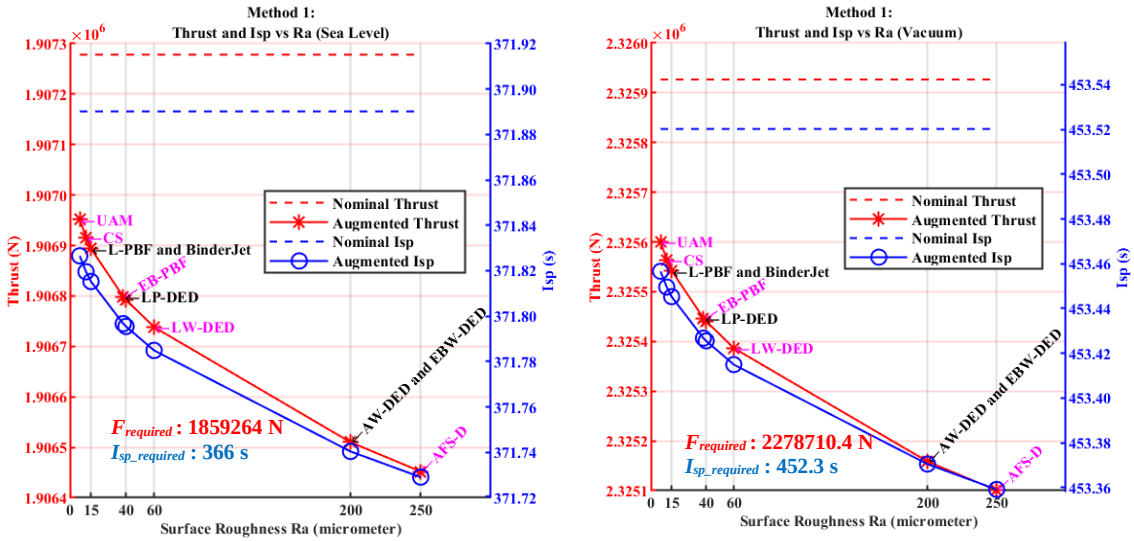

Figure 14. A) *F* and I_{sp} variations in sea-level for Energy Balance Method **B)** *F* and I_{sp} variations in vacuum for Energy Loss Method. (Nominal – no losses and Augmented – accounting for losses). Screened out processes are highlighted pink [39].

A. **B.**

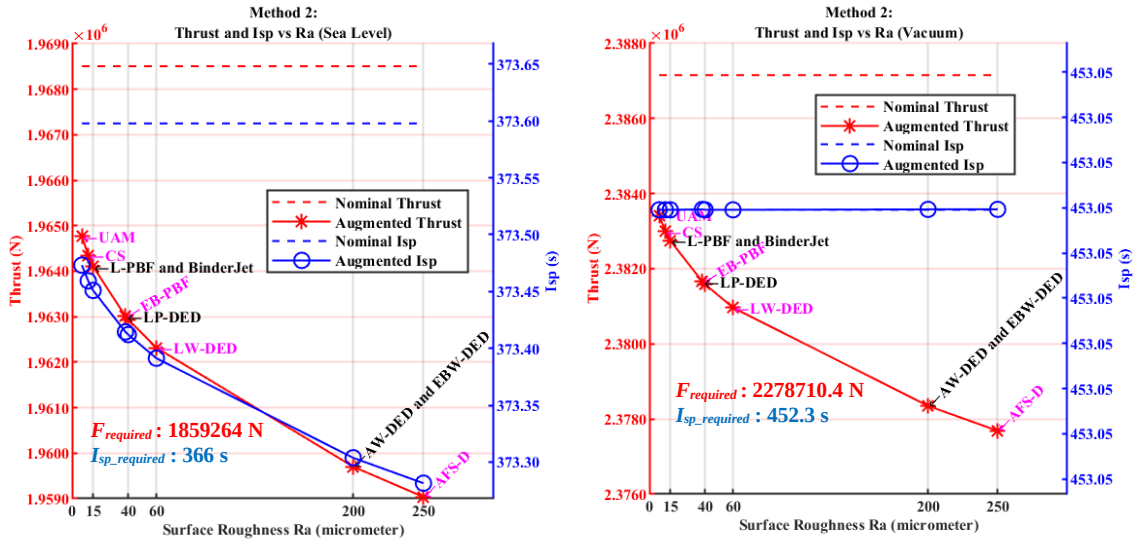

Figure 15 A) F and I_{sp} variations in sea-level for Direct Pressure Loss Method **B)** F and I_{sp} variations in vacuum for Direct Pressure Loss Method. (Nominal – no losses, and Augmented – accounting for losses) [39]. Screened out processes are highlighted pink.

A. **B.**

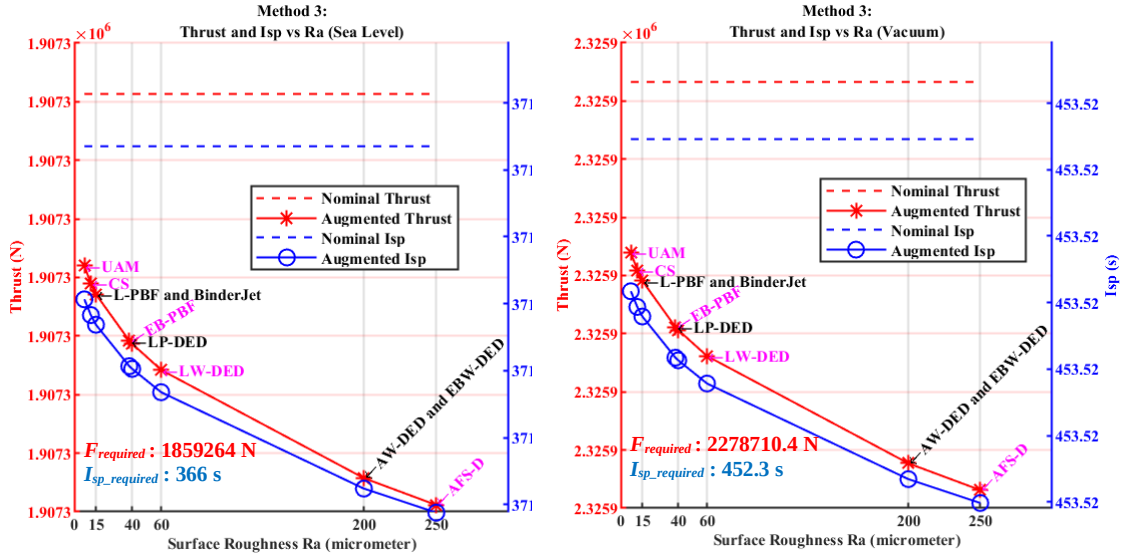

Figure 16 A) F and I_{sp} variations in sea-level for Fanno Flow Method **B)** F and I_{sp} variations in vacuum for Fanno Flow Method. (Nominal – no losses, and Augmented – accounting for losses) [39]. Screened out processes are highlighted pink.

As physically expected, the AM processes with the highest surface roughness (DED and AFS-D) showed the most loss in performance, however, the losses are smaller than expected. To show how small the losses in performance are, the percent difference was calculated for each method at each surface roughness and are depicted in Table 13, Table 14, and Table 15.

Table 13. % difference between nominal performance values and augmented values using Method 1. Screened out processes are highlighted pink.

	Energy Loss Method			
	Thrust		***Isp***	
	% loss SL	**% loss Vac**	**% loss SL**	**% loss Vac**
UAM	0.017	0.014	0.017	0.014
CS	0.019	0.016	0.019	0.016
L-PBF	0.020	0.017	0.020	0.017
Binder Jet	0.020	0.017	0.020	0.017
EB-PBF	0.025	0.021	0.025	0.021
LP-DED	0.025	0.021	0.025	0.021
LW-DED	0.028	0.023	0.028	0.023
AW-DED	0.040	0.033	0.040	0.033
EBW-DED	0.040	0.033	0.040	0.033
AFS-D	0.043	0.036	0.043	0.036

Table 14. % difference between nominal performance values and augmented values using Method 2. Screened out processes are highlighted pink.

	Direct Pressure Loss Method			
	Thrust		***Isp***	
	% loss SL	**% loss Vac**	**% loss SL**	**% loss Vac**
UAM	0.190	0.157	0.033	0.000
CS	0.211	0.174	0.037	0.000
L-PBF	0.224	0.185	0.039	0.000
Binder Jet	0.224	0.185	0.039	0.000
EB-PBF	0.279	0.230	0.049	0.000
LP-DED	0.283	0.233	0.050	0.000
LW-DED	0.314	0.259	0.055	0.000
AW-DED	0.447	0.369	0.079	0.000
EBW-DED	0.447	0.369	0.079	0.000
AFS-D	0.481	0.397	0.085	0.000

Table 15. % difference between nominal performance values and augmented values using Method 3. Screened out processes are highlighted pink.

	Fanno Flow Method			
	Thrust		***Isp***	
	% loss SL	**% loss Vac**	**% loss SL**	**% loss Vac**
UAM	0.0003	0.0003	0.0003	0.0003
CS	0.0003	0.0003	0.0003	0.0003
L-PBF	0.0004	0.0003	0.0004	0.0003
Binder Jet	0.0004	0.0003	0.0004	0.0003
EB-PBF	0.0004	0.0004	0.0004	0.0004
LP-DED	0.0004	0.0004	0.0004	0.0004
LW-DED	0.0005	0.0004	0.0005	0.0004
AW-DED	0.0007	0.0006	0.0007	0.0006
EBW-DED	0.0007	0.0006	0.0007	0.0006
AFS-D	0.0007	0.0006	0.0007	0.0006

While all three methods yielded similar trends with the percentage losses all falling below 1 percent, the performance loss at sea level was highest when utilizing the Direct Pressure Loss Method (Method 2). However, this method showed negligible losses in Isp in vacuum values Figure 15 B) and Table 14. This difference in losses can be attributed to how the pressure loss is implemented in each method. Energy Balance Method directly calculates the exit velocity from the first law of thermodynamics, without manipulating the chamber pressure and mass flowrate. However, Direct Pressure Loss Method recalculates mass flow rate based on the new chamber pressure. As seen in Equations (3.4) and (3.5), a decrease in the mass flowrate results in loss in thrust, as thrust is dependent on mass flow rate. This results in virtually no drop in I_{sp} in vacuum using Direct Pressure Loss Method.

The Fanno Flow Method shows negligible losses to thrust and Isp for both sea level and vacuum conditions, Figure 16 and Table 15. This can be attributed to the consideration of only the constant area section of the geometry which is around 5.22 inches in comparison to overall geometry which is of length around 24.290 inches [40]. Pressure loss is inversely proportional to diameter as seen in Equation (3.16). Since the constant area portion part of

the LT-MCC has the largest diameter, this would also contribute to the performance drops being the lowest. Therefore, the losses estimated are smaller and have a negligible impact on performance.

To gain another perspective on how these pressure losses affect performance, another means of comparing the relative performance can be used that is not dependent on nozzle geometry or ambient conditions. Characteristic velocity (c^*) is quick calculation which is used to compare the relative performance of different chemical rocket propulsion system designs and propellants [44]. Characteristic velocity is defined by Equation (4.20) [44]:

$$c^* = p_1 A_t / \dot{m} \,. \tag{4.20}$$

The percent losses in characteristic velocity for each of the methods are displayed in Table 16.

Table 16. % loss in characteristic velocities for each method. Screened out processes are highlighted pink.

	% Loss: Energy Loss Method	% Loss: Direct Pressure Loss Method	% Loss: Fanno Flow Method
UAM	0.157	0.156	0.007
CS	0.174	0.172	0.007
L-PBF	0.185	0.182	0.008
Binder Jet	0.185	0.182	0.008
EB-PBF	0.230	0.224	0.009
LP-DED	0.233	0.227	0.009
LW-DED	0.259	0.251	0.010
AW-DED	0.369	0.351	0.015
EBW-DED	0.369	0.351	0.015
AFS-D	0.397	0.377	0.016

When nozzle geometry and ambient conditions are not considered, the relative performance, shown in Table 16 as characteristic velocity, shows comparable losses when comparing the Energy Loss Method and the Direct Pressure Loss Method (within 5%). This lends credence to the idea that the discrepancy between the losses calculated from these two methods observed in Table 13, Table 14, and Table 15 are due to assumptions downstream of the LT-MCC rather than the actual pressure loss calculations. The characteristic velocities for Fanno flow, however, still show negligible losses in relative performance.

Overall, all three methods display similar trends when examining performance verses surface roughness, however there is a discrepancy between all three methods when comparing the actual losses as seen in Table 13, Table 14, and Table 15. As mentioned in the previous paragraph, these discrepancies can be attributed to the assumptions about area and mass flow rate, but it does present a limitation when using these methods. Future work should develop these three methods further and attempt to eliminate some of the assumptions used in these methods. The general trend evident from these data is that rocket performance in the hot gas side of the LT-MCC tends to decrease as the surface roughness increases on the hot gas wall of the LT-MCC, however, the losses observed showed negligible losses in performance (*Isp, Thrust*).

Once the model was run in SysML and all ten instances of the LT-MCC were generated, none of the performance requirements were flagged as violated. This ability of the model to automate requirement verification proves advantageous for two main reasons. One, when working with a complex system with potentially hundreds of requirements, it can be cumbersome to perform system verification without this automation. Second,

automating this process through MBSE can improve the accuracy of system verification by making it more difficult to miss important information when conducting analyses on a complex system.

4.4 Discussion of Results

The qualitative analysis succeeded in suggesting a recommendation for the best AM option given a candidate part. In doing so, a rank order of all the AM options was established giving the decision maker insight into areas of improvement for the other AM options. The quantitative analysis provides a mathematical relationship between surface roughness inside the LT-MCC and the thrust and I_{sp} of the RS-25 engine. The goal of the analyses performed and subsequent results are to help inform decisions regarding an AM upgrade scenario while using RS-25 as a design example.

4.4.1 Qualitative Analysis

The results for these scenarios indicate L-PBF was the best option for the RS-25 upgrade scenario. Limitations of this methodology lie in the *trade criteria* used to set up the decision matrix. The weights for each *trade criteria* and the scores for each AM process are based on a simple scale which will vary based on the opinion of the decision maker. This methodology, in its present form, could therefore be improved; methods for such improvements will be discussed in Chapter 5. However, as more data become available and as methods for quantifying these *trade criteria* become more robust, there will be precedent to improve the presented methodology. Given the questionable objectivity of this type of decision-making process, more quantitative measures should be implemented to conduct more thorough trade studies on the system. This justifies the use of a physics

based mathematical model to analyze one of the trades, that being surface roughness, which was done in Section 3.2 of Chapter 3.

There are other more robust decision-making methods used in industry such as Analytical Hierarchy Process (AHP) [50] and Utility Analysis [51] that were not used for the trade study in this thesis. Given however, this is an ongoing effort, they will be considered in future study as this process is improved. The primary advantage to using these methods rather than a decision matrix is how they track consistency as the trade study is being conducted. This would eliminate the need for the decision maker to constantly check their consistency when assigning weights and scores.

It is worthy to note, the SE methodology presented assumes that the design of the part (RS-25 or an NTP engine) is subject to minimal changes. This methodology, however, needs refinement in cases of the rocket engine design being driven by AM such as Rocket Lab's Rutherford Engine, and SpaceX's Raptor Engine. If the part design can be traded against AM properties, there exists an opportunity to move aspects of *screening criteria* to *trade criteria* to refine the presented SE-methodology. Additionally, the model-based framework would need to be refined to accommodate the changes in the SE methodology.

4.4.2 Quantitative Analysis

The results using each method were compared and generally showed a slight reduction in performance if the LT-MCC were to be produced using AM. While the expected outcome from the analysis closely matched what was physically expected, there are further considerations which should be accounted for in future work. The first of these is to improve the Fanno Flow Method, which was only briefly touched upon in this study. Higher fidelity models need to be developed to account for varying geometry and high-

speed flows. The second is the incorporation of heat transfer when performing the Energy Balance Method. This study assumed adiabatic flow, which assumes zero heat transfer. This allowed for the heat flux term (*dq*) of Equation (3.12) to be considered negligible, however, in a practical scenario, this heat flux at the boundary of the combustion chamber would result in an additional loss in KE at the exit and result in significant reduction in performance. Future work on this model should seek to incorporate energy losses due to both the work done by the expanding gases due to skin friction and the heat flux which will increase due to higher surface roughness. Consequently, this will provide a clearer picture of losses and whether they are able to meet the requirements by performing the analysis in *SysML*. While surface roughness is important to consider when assessing the trade-offs of using AM, it is not the only aspect of AM to consider. Properties such as yield strength and heat transfer are among some of the other aspects of AM that must also be considered to make an informed decision regarding whether to use AM or not. In the previous sections of this Thesis (Chapter 2, Chapter 3), these instances have been briefly discussed.

4.5 Summary of Results

The results of both the qualitative analysis (Section 4.1) and the quantitative analysis (Section 4.2) fit inside the overall trade space for assessing AM for the RS-25 in the following ways. The qualitative analysis provides the decision factors, the weight criteria, the viable candidates, and scores for the candidates, which are necessary steps in a general trade study process and map well with steps illustrated in [32]. Similarly, the results output from the quantitative analysis indicates how printing the component and changing the AM process will affect performance. This aids in the evaluation of all the viable candidates and helps the decision maker make a more informed decision regarding

AM for rocket engines. Outputting the results of this (and future) analysis allows for the automation of requirements verification all throughout the trade study.

Chapter 5. Conclusions

5.1 Discussion of Research Question

The literature review in Chapter 2 revealed the need to develop cost effective strategies for the RS-25 in order to meet the future launch manifest of Artemis missions. It was shown that the majority of the development costs for the SSME were spent in the TFF cycle largely due to elimination of failure modes. Previous work on this topic sought to develop cost-effective test strategies by understanding failure modes better before testing the engine thus minimizing the amount of time spent in TFF and decreasing the cost of the engine. The work done in this thesis showed that AM has seen much expanded use in recent years as a method for potential cost and lead time savings. However, these potential benefits have to be offset against the potential shortcomings of AM in order to make informed decisions in an engine upgrade scenario. This led to the research questions posed in Chapter 2, which are restated here.

Research Questions

How is LRE performance affected by AM, specifically surface roughness?

How can MBSE aid in LRE Affordability?

To answer these questions, a brief overview of the different AM processes from the literature [2], [6], [3] were summarized. This included a short description of each primary AM process, as well as benefits and detriments of AM. Furthermore, a brief overview of MBSE was presented along with a review of the previous work done and how this paper

fits into the scope of the affordability research. A SE methodology was presented for deciding between AM and CM by first screening out the impossible AM processes (based on the *screening criteria*), then performing a trade study using *trade criteria* to score the AM processes and CM process. The information Gradl *et al.* [1], [11], [12] provides is tremendously informative and invaluable for any decision maker attempting to select additive or conventional manufacturing. The numerous choices for AM, the number of selection criteria, and the interdependency of many of selection criteria, however, can make the decision between AM and conventional quite strenuous. One of the goals of this research was to transform the selection criteria into a simple SE based methodology and apply it to a model-based affordability framework.

The results from the screening process and decision matrix method expressed in Section 4.1 showed that in an AM upgrade scenario, L-PBF was the most suited option for the LT-MCC. The results from the analyses relayed in this section will assist in the development of a methodology which can assess the viability and utility of AM parts for the RS-25, its production restart, and recertification. As the model-based approach in generally suited for multiple rocket engine architectures, these techniques can also be applied to other LREs, and advanced systems such as Nuclear Thermal Propulsion (NTP) [37].

To demonstrate how this methodology and model-based affordability framework can be expanded upon and further quantified, a mathematical model for analyzing surface roughness effects on engine performance was created. As seen in Section 3.2, *MATLAB*® subroutines were created to evaluate the losses and performance and run through the model-based framework developed in *SysML*. This model was then verified using SSME

data [46]. Three methods for recalculating performance given pressure loss were developed and presented.

In doing this study, a better understanding of the trade-offs between upgrading a rocket engine component with AM and rocket performance was gained. The capabilities of a model-based approach were also demonstrated. In an affordability context, requirement traceability is vital if engineers are to make well-informed decisions. For instance, a manufacturing engineer with this model could better estimate how much post processing is necessary for an AM part to satisfy a requirement. This could cut down the lead time of the part even further, or alleviate potential failures on the test stand, therefore decreasing the time to certify the engine. Like Section 3.1, this analysis seeks to establish a comprehensive model-centric approach for affordability ensuring traceability and consistency throughout the life-cycle of the system.

5.2 Contributions

The work presented in this thesis offers three contributions to the investigation of AM for rocket engine development. These contributions fit well inside the RS-25 affordability framework as seen in Figure 1 and Figure 2, in which the *Test Engine* use-case was developed in previous work, and the work done in this thesis develops the *Upgrade Engine* use-case.

The first contribution is the SE approach of assessing AM benefits for rocket engine presented in Section 3.1. It offers decision makers a quick recommendation for whether to print a rocket engine component or to fabricate it traditionally. This also fits well into the development of a model-based affordability framework for the rocket engine development. If AM is the best option, it indicates which AM process is viable for a component instance,

and which ones can be disregarded by design, this methodology will evolve as more data on AM are realized.

The second contribution is the surface roughness analysis conducted in Section 3.2. This analysis mathematically links surface roughness in the LT-MCC gas end to rocket engine performance. While this analysis is governed by underlining assumptions regarding the physics of a LRE, it does provide a means to estimate how engine performance is affected by AM in an upgrade engine scenario.

The third contribution is the implementation of this methodology in *SysML* as seen in Section 3.3. While for a single analysis as presented in this thesis, the implementation of MBSE may seem trivial, as the analyses gain complexity and become harder to manage, this contribution gains utility. The automation of systems engineering tasks in this case will help envision failure-centric aspects early in the life-cycle of the system, optimizing the time spent in test-fail-fix cycle, delivering affordability.

5.3 Future Work

The research presented in this thesis is part of an ongoing effort to deliver affordability to the RS-25 engines and other LRE, and it will continue after this work is published. That being said, there are ways in which this work could be expanded upon or improved. One area of expansion which was alluded to multiple times previously is the addition of other analyses which could be integrated into the existing framework and further inform decision making for AM. Examples of these analyses using the same component used in this thesis (LT-MCC) would be an analysis of the regeneratively cooled passages and a structural analysis of the component given the increased porosity inherent in most metal AM parts. The former of these would be the most viable to pursue in future

work as the analysis would use similar physical principles to the ones presented in this thesis. The later of these analyses would take time to develop as microstructure formations in metals are difficult to model as seen in [28].

An area where this work could be improved is the validation of the data output from the models presented in this thesis. Work could be done to confer with subject matter experts to determine how accurate the qualitative work/results (Section 4.1) are as well as the qualitative results (Section 4.2). This could be done in multiple ways. Firstly, a dialogue could be established directly with AM engineers who work on LREs, and the results could be compared to their experience and engineering common sense. Secondly, the output of the analysis could be compared to data collected from testing other AM LRE components. While AM failure data are limited, this would still do much to establish a baseline for making informed decisions when considering AM for affordability purposes.

Future work should also seek to address the numerous assumptions made in the methodology section of this thesis, particularly in Section 3.1, which outlines the underlining assumptions surrounding the screening process. These assumptions do not take into consideration bimetallic AM process, *i.e.*, processes which can print using two materials. This is a particularly useful capability which NASA has tested and plans to implement in future projects [2]. Future work could also dive into the specific vendors which provide these AM machines, as this thesis assumes all machines of the same type of AM have negligibly different capabilities. In reality, there is significant variation between venders, and future work could expand the trade space to include the various vendors [2].

The implementation of the SE methodology into the *SysML* models presented in this thesis is currently being evaluated. While the analysis presented in Section 3.2 is fully

captured and automated in *SysML*, the screening process and decision matrix are not. A fully automated model of these processes would further aid in the development of the affordability framework shown in Figure 1.

References

[1] Davidson, M. RS-25: The Clark Kent of Engines for the Space Launch System. *nasa.gov*. https://www.nasa.gov/exploration/systems/sls/rs25-engine-powers-sls.html.

[2] Gradl, P., Tinker, D. C., Park, A., Mireles, O. R., Garcia, M., Wilkerson, R., and Mckinney, C. "Robust Metal Additive Manufacturing Process Selection and Development for Aerospace Components." *Journal of Materials Engineering and Performance*, No. April, 2022. https://doi.org/10.1007/s11665-022-06850-0.

[3] Gradl, P. R., Greene, S. E., Protz, C., Bullard, B., Buzzell, J., Garcia, C., Wood, J., Cooper, K., Hulka, J., and Osborne, R. "Additive Manufacturing of Liquid Rocket Engine Combustion Devices: A Summary of Process Developments and Hot-Fire Testing Results." *2018 Joint Propulsion Conference*, Vol. 2018, 2018, pp. 1–34. https://doi.org/10.2514/6.2018-4625.

[4] Gradl, P. R., Teasley, T. W., Protz, C. S., Katsarelis, C., and Chen, P. "Process Development and Hot-Fire Testing of Additively Manufactured NASA HR-1 for Liquid Rocket Engine Applications." *AIAA Propulsion and Energy 2021 Forum*, 2021, pp. 1–23. https://doi.org/10.2514/6.2021-3236.

[5] Clinton, J., Raymond, Prater, T., Morgan, K., and Ledbetter, F. "NASA Additive Manufacturing Initiatives for Deep Space Human Exploration." *69th International Astronautical Congress (IAC);MSFC-E-DAA-TN61658;IAC-18C29*, No. October, 2018, pp. 1–5.

[6] Gradl, P. R., Mireles, O. R., Protz, C. S., and Garcia, C. P. *Metal Additive Manufacturing for Propulsion Applications*. AIAA, American Institute of Aeronautics and Astronautics, Incorporated, 2022.

[7] Havskjold, G. "Developing Innovative Products on Budget and On Schedule–Part 1: Identifying and Measuring Cost Drivers Correlates Technical Uncertainty with Rework Cycles." *45th AIAA/ASME/SAE/ASEE Joint Propulsion Conference & Exhibit*, 2009. https://doi.org/10.2514/6.2009-5436.

[8] Aldrich, D. E. "Study to Accelerate Development by Test of a Rocket Engine." *Rocketdyne Report R-8099, NASA-18734*, 1969.

[9] Joyner, C., Laurie, J., Levack, D., and Zapata, E. "Pros, Cons, and Alternates to Weight Based Cost Estimating." *47th AIAA/ASME/SAE/ASEE Joint Propulsion Conference & Exhibit*, 2011. https://doi.org/10.2514/6.2011-5502.

[10] Bower, A. *THE EFFECTS OF STRUCTURAL MARGIN IN THE TEST-FAIL-FIX CYCLE FOR ROCKET ENGINES*. University of Alabama in Huntsville, 2019.

[11] Holladay, J. B., Knizhnik, J., Weiland, K. J., Stein, A., Sanders, T., and Schwindt, P. “MBSE Infusion and Modernization Initiative (MIAMI): ‘Hot’ Benefits for Real NASA Applications.” *2019 IEEE Aerospace Conference*, Vols. 2019-March, 2019, pp. 1–14. https://doi.org/10.1109/AERO.2019.8741795.

[12] Evans, J., Cornford, S., and Feather, M. S. “Model Based Mission Assurance: NASA’s Assurance Future.” *2016 Annual Reliability and Maintainability Symposium (RAMS)*, Vols. 2016-April, 2016, pp. 1–7. https://doi.org/10.1109/RAMS.2016.7448047.

[13] Huang, Z., Hansen, R., and Huang, Z. “Toward FMEA and MBSE Integration.” *2018 Annual Reliability and Maintainability Symposium (RAMS)*, Vols. 2018-Janua, 2018, pp. 1–7. https://doi.org/10.1109/RAM.2018.8463084.

[14] Izygon, M., Wagner, H., Okon, S., Wang, L., Sargusingh, M., and Evans, J. “Facilitating R&M in Spaceflight Systems with MBSE.” *2016 Annual Reliability and Maintainability Symposium (RAMS)*, Vols. 2016-April, 2016, pp. 1–6. https://doi.org/10.1109/RAMS.2016.7448031.

[15] Groen, F. J., Evans, J. W., and Hall, A. J. “A Vision for Spaceflight Reliability: NASA’s Objectives Based Strategy.” *2015 Annual Reliability and Maintainability Symposium (RAMS)*, Vols. 2015-May, 2015, pp. 1–6. https://doi.org/10.1109/RAMS.2015.7105106.

[16] Friedenthal, S., Moore, A., and Steiner, R. *A Practical Guide to SysML: The Systems Modeling Language*. Morgan Kaufmann, Waltham, MA, MA, 2015.

[17] RS-25 Engine Data Sheet. *rocket.com*. https://www.rocket.com/space/liquid-engines/rs-25-engine.

[18] Honeycutt, J., Cianciola, J. C., Blevins, J., Heflin, J., Tiller, B., and Reynolds, D. C. NASA Space Launch System Completes Green Run Testing, Begins Assembly. 2021.

[19] Honeycutt, J., Cianciola, C., Blevins, J., and Burkey, M. “NASA’s Space Launch System Progress Toward the Launch Pad.” *AIAA Propulsion and Energy 2020 Forum*, 2020. https://doi.org/10.2514/6.2020-3533.

[20] Vetcha, N., Strickland, M. B., Philippart, K. D., and Giel, T. V. “Overview of RS-25 Adaptation Hot-Fire Test Series for SLS, Status and Lessons Learned.” *2018 Joint Propulsion Conference*, 2018. https://doi.org/10.2514/6.2018-4459.

[21] Ballard, R. O. “Next-Generation RS-25 Engines for the NASA Space Launch System.” *7th European Conference for Aeronautics and Space Sciences (EUCASS 2017)*, 2017.

[22] Thompson, C. L. NASA Continues Testing Redesigned Artemis Moon Rocket Engines. *nasa.gov*.

https://www.nasa.gov/centers/stennis/news/releases/2023/NASA-Continues-Testing-Redesigned-Artemis-Moon-Rocket-Engines.

[23] Bower, A. J., and Thomas, D. “An Affordability Model Framework for the RS-25 Liquid Rocket Engine.” *2018 Joint Propulsion Conference*, 2018, pp. 1–9. https://doi.org/10.2514/6.2018-4460.

[24] Kraft, R. NASA to Stand Down on Artemis I Launch Attempts in Early September, Reviewing Options. *blogs.nasa.gov*. https://blogs.nasa.gov/artemis/2022/09/03/nasa-to-stand-down-on-artemis-i-launch-attempts-in-early-september-reviewing-options/.

[25] Lakshmipuram Raghu, S., and Thomas, L. “Modeling Behavior Elements for the RS-25 Engine Using SysML for Improved Affordability.” *AIAA Propulsion and Energy 2021 Forum*, 2021, pp. 1–12. https://doi.org/10.2514/6.2021-3578.

[26] Lakshmipuram Raghu, S., and Thomas, L. D. “Model Based Failure Mode, Effects and Criticality Analysis (MBFMECA) for the RS-25 Engine Using SysML.” *AIAA Scitech 2021 Forum*, 2021. https://doi.org/10.2514/6.2021-0305.

[27] Raghu, S. L., Tudor, M., Thomas, L. D., and Wang, G. “MBSE Utilization for Additive Manufactured Rocket Propulsion Components.” *2022 IEEE Aerospace Conference*, 2022, p. wasson. https://doi.org/10.1109/AERO53065.2022.9843586.

[28] Rodgers, T. M., Madison, J. D., and Tikare, V. “Simulation of Metal Additive Manufacturing Microstructures Using Kinetic Monte Carlo.” *Computational Materials Science*, Vol. 135, 2017, pp. 78–89. https://doi.org/10.1016/j.commatsci.2017.03.053.

[29] Mankins, J. C. *TECHNOLOGY READINESS LEVELS A White Paper*. 1995.

[30] Peters, S. “A Readiness Level Model for New Manufacturing Technologies.” *Production Engineering*, Vol. 9, Nos. 5–6, 2015, pp. 647–654. https://doi.org/10.1007/s11740-015-0636-5.

[31] Waller, J. M., Parker, B. H., Hodges, K. L., Burke, E. R., and Walker, J. L. “Nondestructive Evaluation of Additive Manufacturing State-of-the-Discipline Report.” *NASA/TM-2014-218560*, No. November, 2014, pp. 1–36.

[32] Wasson, C. S. *System Engineering Analysis, Design, and Development*. Wiley.

[33] Department of Defense. *Systems Engineering Fundamentals*. CreateSpace Independent Publishing Platform, 2016.

[34] Jue, F., and Kuck, F. “Space Shuttle Main Engine (SSME) Options for the Future Shuttle.” *38th AIAA/ASME/SAE/ASEE Joint Propulsion Conference & Exhibit*, 2002. https://doi.org/10.2514/6.2002-3758.

[35] *NASA Systems Engineering Handbook*. NASA SP-2016- 6105 Rev2, 2016.

[36] Nash, A., and Austin, A. "Methods for Determining Initial Feasibility: Identify the Accessibile Trade Space." *2023 IEEE Aerospace Conference*, 2023.

[37] Buettner, J., Raghu, S. L., Aueron, A., Rawlins, S., and Thomas, L. D. "A System Engineering Approach to Assess the Benefits of Additive Maufacturing for Rocket Engines." *2023 IEEE Aerospace Conference*, 2023. https://doi.org/10.1109/AERO55745.2023.10115942.

[38] Adams, T., Grant, C., and Watson, H. "A Simple Algorithm to Relate Measured Surface Roughness to Equivalent Sand-Grain Roughness." *International Journal of Mechanical Engineering and Mechatronics*, 2012. https://doi.org/10.11159/ijmem.2012.008.

[39] Buettner, J., Lakshmipuram Raghu, S., and Thomas, L. "Understanding the Benefits of Utilizing Additive Manufacturing (AM) for Liquid Rocket Engine Components and Its Quantification Using Model-Based Systems Engineering (MBSE)." *2023 AIAA SciTech Forum*, 2023. https://doi.org/10.2514/6.2023-1896.

[40] Kibler, L. Get the Facts On… Surface Roughness. *ge.com*. https://www.ge.com/additive/blog/get-facts-surface-roughness. Accessed Nov. 15, 2022.

[41] C. B. Carolo, L., and Cooper O., R. E. "A Review on the Influence of Process Variables on the Surface Roughness of Ti-6Al-4V by Electron Beam Powder Bed Fusion." *Additive Manufacturing*, Vol. 59, 2022, p. 103103. https://doi.org/10.1016/j.addma.2022.103103.

[42] Ahn, D. "Directed Energy Deposition (DED) Process: State of the Art." *International Journal of Precision Engineering and Manufacturing- Green Technology*. https://doi.org/10.1007/s40684-020-00302-7.

[43] Dehoff, R. R., and Babu, S. S. "Characterization of Interfacial Microstructures in 3003 Aluminum Alloy Blocks Fabricated by Ultrasonic Additive Manufacturing." *Acta Materialia*, Vol. 58, No. 13, 2010, pp. 4305–4315. https://doi.org/10.1016/j.actamat.2010.03.006.

[44] Sutton, G. P., and Biblarz, O. *Rocket Propulsion Elements*. Wiley, 2016.

[45] White, F. M. *Fluid Mechanics*. McGraw Hill Education.

[46] Nickerson, G. R., and Dang, L. D. *Performance Predictions for an SSME Configuration with an Enlarged Throat*. 1985.

[47] Heister, S. D., Anderson, W. E., Pourpoint, T. L., and Cassady, R. J. *Rocket Propulsion*. Cambridge University Press, 2019.

[48] Brady, B. Space Shuttle Main Engine Computational Model. *Cryo-Rocket.com*. https://www.cryo-rocket.com/flow-model/5.3-compressible-flow/.

[49] Analyzing Flow with Friction Through an Insulated Constant Area Duct. *MathWorks*. https://www.mathworks.com/help/aerotbx/ug/analyzing-flow-with-friction-through-an-insulated-constant-area-duct.html.

[50] Triantaphyllou, E., and Mann, S. H. "USING THE ANALYTIC HIERARCHY PROCESS FOR DECISION MAKING IN ENGINEERING APPLICATIONS: SOME CHALLENGES." *Journal of Industrial Engineering: Applications and Practice*, Vol. 2, No. 1, 1995, pp. 35–44.

[51] Garrett, C. J., Levack, D. J. H., and Rhodes, R. E. "Using Technical Performance Measures." *47th AIAA/ASME/SAE/ASEE Joint Propulsion Conference & Exhibit*, 2011. https://doi.org/10.2514/6.2011-5500.

Appendix A. *MATLAB*® Code

Main *MATLAB*® Script

```
%% Start here
clear;
close all;
% this code will calculate the geometry of the MCC of SSME
% This code will calculate the pressure loss due to the surface
roughness
% This code will calculate the ne Thrust and Isp of the SSME due to
pressure

%% Required Functions:
    %MCC_geometry
    %coolprop
    %delta_p
    %performance

%import py.CoolProp.CoolProp.PropsSI
addpath('Y:\Nuclear Thermal Propulsion Stage\Cool Prop'); %Office PC

%% Constants

in2m = 0.0254 ;
A_t = pi * (5.4417^2) * in2m * in2m ; % [m2]
L = 5.222 ; % [in]

% Operating Conditions

% Chamber Pressure
psia2psi = 14.696; % [psia]
psi2Pa = 6894.757 ; % [N/m2 or Pa]
P_1psia = 3010 ; % [psia] For large throat MCC power level 109 %
% (Nicerson et al. Performance predictions of LTMCC)
P_1psi = P_1psia - psia2psi;
P_1 = P_1psi * psi2Pa; % [Pa]

P_Nick = 3010; % [psia]
P_Nickpsi = P_Nick - psia2psi;
P_NickPa = P_Nickpsi * psi2Pa; % [Pa]

% Chamber Temperature
R2K = (5/9);%[K];
T_1R = 6591.104 ; % [R]For large throat MCC power level 109 %
% (Nicerson et al. Performance predictions of LTMCC)
T_1 = T_1R * R2K ; %[K]
T_1F = convtemp(T_1,'K','F');

T_NickR = 6591.104; % [R]
T_NickK = T_NickR *R2K; % [K]
T_NickF = convtemp(T_NickK,'K','F');

%density
```

```
rho = CoolProp.PropsSI('D','P',P_1,'T',T_1,'Water');
mu = CoolProp.PropsSI('V', 'P', P_1,'T',T_1, 'Water');

%Area Ratio; Nicerson et al.
E = 68.573;

% %CoolProp: Use this if you need to check with coolprop
% Cp = CoolProp.PropsSI('Cpmolar', 'P', P_1, 'T', T_1, 'Water');
% Cv = CoolProp.PropsSI('Cvmolar', 'P', P_1, 'T', T_1, 'Water');
% k = Cp/Cv;
% MW = CoolProp.PropsSI('molar_mass', 'P', P_1, 'T', T_1, 'Water');
% Ru = CoolProp.PropsSI('gas_constant', 'P', P_1, 'T', T_1, 'Water');
% R = Ru/MW;

% Thermodynamics: From Utah State Lecture: Sample calculations
k = 1.2; %specific heat ratio
MW = 13.6;%kg/kg-mol (get from coolprop)
Ru = 8314; %universal gas constant in J/kg-mol-K
R = Ru/MW; %gas constant

%m_dot = massflow(A_t,P_1,k,R,T_1); %get mass flow rate
lb2kg2 = 2.205;
m_dot = 1152.760/lb2kg2; %Nickerson et al.
%m_dot = massflow(A_t,P_1,k,R,T_1);

%import roughness values
% filename = 'SciTech Data.xlsx';
%roughness = readcell(filename,'Range','C3:C12');
roughness = [15,38,40,60,200,200,7,250,11.5,15]; %roughness values

%% Calculations
for i = 1:length(roughness)

    Geometry = MCC_geometry(0.1); %get nozzle geometry
    %[P1_new,deltaP] = fanno(P_1, T_1,k,rho,mu,roughness(i),m_dot,L);
    [rho,mu,Re,Mach,deltaP(i)] =
delta_p_Eloss(Geometry,roughness(i),m_dot,P_1,T_1); %get pressure loss

    [Thrust(i,:), Isp(i,:), ThrustVac(i,:), IspVac(i,:), C_f(i,:),
C_fVac(i,:)] = Performance(m_dot,P_1,T_1,R,k,E,A_t,deltaP(i)); %get
performance

end

%Energy Balance Method
% Data =
table(deltaP.',Thrust(:,1),Thrust(:,2),ThrustVac(:,1),ThrustVac(:,2),Is
p(:,1),Isp(:,2),IspVac(:,1),IspVac(:,2)); %table with all values
% writetable(Data,filename,'Range','D3:L12','WriteVariableNames',0)

%Direct Method
% Data =
table(deltaP.',Thrust(:,1),Thrust(:,2),ThrustVac(:,1),ThrustVac(:,2),Is
p(:,1),Isp(:,2),IspVac(:,1),IspVac(:,2)); %table with all values
% writetable(Data,filename,'Range','D16:L25','WriteVariableNames',0)
```

```
ThrustSealbf = convforce(double(Thrust(1,1,1)),'N','lbf'); %double
ThrustVaclbf = convforce(double(ThrustVac(1,1,1)),'N','lbf');


%% Results

%plots Thrust
plotThrust(sort(roughness),roughnessG,Thrust(:,1),Thrust(:,2))


Isp_NickVac = 454.4525 ; % [seconds]
Thrust_NickVaclbf = 523874.7 ; % [lbf]
% Thrust_NickVacN = convforce(Thrust_NickVaclbf,'lbf','N');

%Actual SLS

Isp_SLSVac = 452.3 ; % [seconds]
Isp_SLSsea = 366 ; % [seconds]
Thrust_SLSVac = 512300 ; % [lbf]
Thrust_SLSSea = 418000 ; % [lbf]
P1_SLS = 2994; % [psia]

heading = sprintf('\t\t\t\t\t\t<strong> Performance Model for RS-25
Main Combustion Chamber Assesments (PM_MCC) at 109 percent Power level
- AM Surface Roughness Effects</strong>');
disp(heading);

Results_model = table;
Results_model.Results = ["Nickerson et al. 1985 (TDK/BLM Solution)";
"Actual - SLS Missions"; "PM_MCC (This Model)";];
Results_model.ChamberPressure_psia = [P_Nick ; P1_SLS ; P_1psia];
Results_model.ChamberTemp_degreeF = [T_NickF ;  "NA" ; T_1F];
Results_model.Thrust_SeaLevel_lbf = ["NA" ; Thrust_SLSSea ;
ThrustSealbf];
Results_model.Thrust_Vaccum_lbf = [Thrust_NickVaclbf ; Thrust_SLSVac ;
ThrustVaclbf];
Results_model.Thrust_Coefficient_Sea_Level = ["NA" ; "NA" ;
double(C_f(1))];
Results_model.Thrust_Coefficient_Vacuum = ["NA" ; "NA" ;
double(C_fVac(1))];
Results_model.Isp_SeaLevel_seconds = ["NA" ; Isp_SLSsea ;
double(Isp(1,1,1))];
Results_model.Isp_Vaccum_seconds = [Isp_NickVac ; Isp_SLSVac ;
double(IspVac(1,1,1))];

disp(Results_model);

heading1 =sprintf('\n\t\t\t<strong>Percent Difference - PM_MCC versus
Avialable Data</strong>');
disp(heading1);

Results_model1 = table;
Results_model1.Results = ["Nickerson et al. 1985 (TDK/BLM Solution)";
"Actual - SLS Missions"];
Results_model1.ChamberPressure = [percentdiff(P_1psia,P_Nick) ;
percentdiff(P_1psia,P1_SLS)];
Results_model1.ChamberTemp = [percentdiff(T_1F,T_NickF) ;  "NA"];
```

```
Results_model1.Thrust_SeaLevel = ["NA" ;
percentdiff(ThrustSealbf,Thrust_SLSSea)];
Results_model1.Thrust_Vaccum =
[percentdiff(ThrustVaclbf,Thrust_NickVaclbf) ;
percentdiff(ThrustVaclbf, Thrust_SLSVac)];
Results_model1.Isp_SeaLevel = ["NA" ;
percentdiff(double(Isp(1,1,1)),Isp_SLSsea)];
Results_model1.Isp_Vaccum =
[percentdiff(double(IspVac(1,1,1)),Isp_NickVac) ;
percentdiff(double(IspVac(1,1,1)),Isp_SLSVac)];
disp(Results_model1);
```

MATLAB® Functions (Subroutines)

```
function MCC_Coordinates = MCC_geometry (step_size)
    % clear;
    % close all;
    % clc;
    %Created by: Josh Buettner
    %Last Edited: 11/4/22
    %In association with CSIL and UAH
    %% Constants
    %radii
    R_injector = 9.425;  % inches
    r_1 = 2.688; % radii injector side (converging) [inches]
    r_2 = 9.464; % radii leading towards throat [inches]
    r_3 = 1.088; % radii expansion side (diverging) [inches]

    %length intervals starting from the injector end
    L_1 = 5.222; % point_1 x-coordinate
    L_2 = 6.456579; % point_2 x-coordinate
    L_3 = 11.16;% point_3 x-coordinate
    L_4 = 15.222;% point_4 x-coordinate
    L_5 = 15.87677475; % point_5 x-coordinate
    L_6 = 24.290;% point_6 x-coordinate
    %% Equations
    % A = 9.425;
    % B = r_1 * sqrt(1 - (((x(i)-5.22)/r_1)^2)) + 6.737;
    % C =  -0.5882934166*x(i) + 12.92307289; %derived equation
    % D = -r_2 * sqrt(1 - (((15.222-x(i))/r_2)^2)) + 14.9057;
    % E = -r_3 * sqrt(1 - (((x(i)-15.222)/r_3)^2)) + 6.530;
    % F = y(i) = 0.6995195368*x(i) - 5.445329549;
    %% Calculations
    x = 0:step_size:L_6;
    y = zeros(1,length(x)); % pre-allocation
    for i = 1:length(x)
        if x(i) >= 0 && x(i) < L_1
            y(i) = R_injector;
        elseif x(i) >= L_1 && x(i) < L_2
            y(i) = r_1 * sqrt(1 - (((x(i)-5.22)/r_1)^2)) + 6.737;
        elseif x(i) >= L_2 && x(i) < L_3
            y(i) = -0.5882934166*x(i) + 12.92307289;
        elseif x(i) >= L_3 && x(i) < L_4
```

```
            y(i) = -r_2 * sqrt(1 - (((15.222-x(i))/r_2)^2)) + 14.9057;
        elseif x(i) >= L_4 && x(i) < L_5
            y(i) = -r_3 * sqrt(1 - (((x(i)-15.222)/r_3)^2)) + 6.530;
        elseif x(i) >= L_5 && x(i) <= L_6
            y(i) = 0.6995195368*x(i) - 5.445329549;
        end
    end
    %% Plots
    % figure (1);
    % plot(x,y,'.-');
    % xlabel('x (in)');
    % ylabel('y (in)');
    % title('MCC Geometry Coordinates')
    % xticks([0 5 10 15 20 L_6]);
    % yticks([0 5 10 15 20 L_6]);
    % ylim([0 11.546]);
    % xlim([0 L_6]);

    MCC_Coordinates = [x' y'];
    save('Geometry.mat', 'MCC_Coordinates');
end

function [A,B,Re,M,delta_p_EL] =
delta_p_Eloss(Geometry,roughness,m_dot,P_1,T_1)
    %clear, clc
    %Josh Buettner
    %Created 10/18/2022
    %last edited: 10/18/2022

    % This methodology is based on previous work done by Hannah Smith
in 2020
        % The assumptions of this analysis are as follows:
        % Saturated liquid oxygen values
        % Constant, cirular cross-sectional
        % No bends in the duct
        % Duct inlet and outlet at the same height
        % Single inlet and single exit
        % Steady state flow
        % Downstream component requires a certain min pressure
    %% Add path to CoolProp
    addpath('Y:\Nuclear Thermal Propulsion Stage\Cool Prop')

    %% constants:
    rho = CoolProp.PropsSI('D','P',P_1,'T',T_1,'Water'); %check this
    mu = CoolProp.PropsSI('V', 'P', P_1,'T',T_1, 'Water'); %get from
coolprop
    R_in = Geometry(:,2); %radius in inches
    L_in = Geometry(:,1); %length in inches
    Ra = roughness;

    %% preliminary Calculation
    L_in = 0.1; %Step size length in inches
    L_m = L_in*0.0245; %Lengh coordinate of each in m
    R_m = R_in*0.0245; %Radius of the MCC in meters
    D = R_m.*2; %diameter of the MCC
    E = 11.03*Ra*(10^-6); %surface roughness converted to relative
roughness for fluid mechanics purposes
```

```
    K = E./D; %ratio of relative roughness to diameter (input into
Colebrook equation below)
    A = pi*((R_m).^2); %area
    A1 = rho*A;
    u = m_dot./(A1); % fluid speed (m/s)
    Re = (rho*u.*D)/mu; %Reynolds number
    speed_of_sound = CoolProp.PropsSI('A','P',P_1,'T',T_1,'Water');
    M = u./speed_of_sound;

    %% Numerical Solver
    %solver
    parfor i = 1:length(Re)
        f_d = sym('f_d');
        Left = 1/(sqrt(f_d));
        Right = -2*log10((K(i)/3.7) + (2.51/(Re(i)*sqrt(f_d))));
%Colebrook eqn.
        fric = vpasolve(Left == Right, f_d, [-Inf Inf]);
        fric2(i)=fric;
        HL(i) = (L_m*fric*(u(i)^2))/(2*D(i)); %head loss
        %PD(i) = (rho*L_m*fric*(u(i)^2))/(2*D(i)); %pressure loss
    end

   A = rho;
   B = mu;

    %Pressure Drop
    delta_p_EL = double(sum(HL)); %Energy balance Method
    %delta_p = double(sum(PD)); %Direct Method

end

function [A,B,Re,M,delta_p_PressureLoss,P1_new] =
delta_p_PLoss(Geometry,roughness,m_dot,P_1,T_1)
    %clear, clc
    %Josh Buettner
    %Created 10/18/2022
    %last edited: 10/18/2022

    % This methodology is based on previous work done by Hannah Smith
in 2020
        % The assumptions of this analysis are as follows:
        % Saturated liquid oxygen values
        % Constant, cirular cross-sectional
        % No bends in the duct
        % Duct inlet and outlet at the same height
        % Single inlet and single exit
        % Steady state flow
        % Downstream component requires a certain min pressure
    %% Add path to CoolProp
    addpath('Y:\Nuclear Thermal Propulsion Stage\Cool Prop')

    %% constants:
    rho = CoolProp.PropsSI('D','P',P_1,'T',T_1,'Water'); %check this
    mu = CoolProp.PropsSI('V', 'P', P_1,'T',T_1, 'Water'); %get from
coolprop
    R_in = Geometry(:,2); %radius in inches
    L_in = Geometry(:,1); %length in inches
```

```
    Ra = roughness;

    %% preliminary Calculation
    L_in = 0.1; %Step size length in inches
    L_m = L_in*0.0245; %Lengh coordinate of each in m
    R_m = R_in*0.0245; %Radius of the MCC in meters
    D = R_m.*2; %diameter of the MCC
    E = 11.03*Ra*(10^-6); %surface roughness converted to relative
roughness for fluid mechanics purposes
    K = E./D; %ratio of relative roughness to diameter (input into
Colebrook equation below
    A = pi*((R_m).^2); %area
    A1 = rho*A;
    u = m_dot./(A1); % fluid speed (m/s)
    Re = (rho*u.*D)/mu; %Reynolds number
    speed_of_sound = CoolProp.PropsSI('A','P',P_1,'T',T_1,'Water');
    M = u./speed_of_sound;

    %% Numerical Solver
    %solver
    parfor i = 1:length(Re)
        f_d = sym('f_d');
        Left = 1/(sqrt(f_d));
        Right = -2*log10((K(i)/3.7) + (2.51/(Re(i)*sqrt(f_d))));
%Colebrook eqn.
        fric = vpasolve(Left == Right, f_d, [-Inf Inf]);
        fric2(i)=fric;
%         HL(i) = (L_m*fric*(u(i)^2))/(2*D(i)); %head loss
        PD(i) = (rho*L_m*fric*(u(i)^2))/(2*D(i)); %pressure loss
    end

   A = rho;
   B = mu;

    %Pressure Drop
%     delta_p = double(sum(HL)); %Energy balance Method
    delta_p_PressureLoss = double(sum(PD)); %Direct Method

end


function [P1_new, Pressure_Loss] = fanno(p_1,T_1,k,rho,mu,Ra,m_dot,L)
R_m = 9.425*0.0254; %Radius of the MCC in meters
    D = R_m*2; %diameter of the MCC
    E = 11.03*Ra*(10^-6); %surface roughness converted to relative
roughness for fluid mechanics purposes
    K = E/D; %ratio of relative roughness to diameter (input into
Colebrook equation below
    A = pi*((R_m)^2); %area
    A1 = rho*A;
    u = m_dot/(A1); % fluid speed (m/s)
    Re = (rho*u*D)/mu; %Reynolds number
    addpath('Y:\Nuclear Thermal Propulsion Stage\Cool Prop'); %Office
PC
    speed_of_sound = CoolProp.PropsSI('A','P',p_1,'T',T_1,'Water');
    M = u/speed_of_sound;
```

```
    f_d = sym('f_d');

    Left = 1/(sqrt(f_d));
    Right = -2*log10((K/3.7) + (2.51/(Re*sqrt(f_d)))); %Colebrook eqn.
    fric = double(vpasolve(Left == Right, f_d, [-Inf Inf]));

%L = 5.222 ; % [in]
in2m = 0.0254 ;
ductLength       = L*in2m;    % Length of the duct [m]
diameter         = D;    % Diameter of the duct [m]
inletMach        = M;     % Mach number at the duct inlet
[dimensionless]
inletPressure    = p_1;     % Static pressure at the duct inlet [kPa]
inletTemperature = T_1;     % Static temperature at the duct input [K]
frictionCoeff    = double(fric);    % Duct friction coefficient
[dimensionless]

fannoParameter = frictionCoeff * ductLength / diameter;

[~, inletTempRatio, inletPresRatio, ~, ~, ~, inletFannoRef] =
flowfanno(k, inletMach);

outletFannoRef = inletFannoRef - fannoParameter;

[outletMach, outletTempRatio, outletPresRatio] = flowfanno(k,
outletFannoRef, 'fannosub');

outletTemperature = inletTemperature / inletTempRatio *
outletTempRatio;

outletPressure = inletPressure / inletPresRatio * outletPresRatio;

M_2f = outletMach       ;
T_2f = outletTemperature ;
P_2f = outletPressure  ;

Pressure_Loss = p_1-P_2f;

P1_new = p_1 - Pressure_Loss;
end


function [Thrust,Isp,ThrustVac,IspVac,C_f,C_fVac] =
Performance(m_dot,p_1,T_1,R,k,E,A_t,delta_p)

    %clear, clc
    %pressure loss effect on thrust and Isp
    %Creator: Josh Buettner
    %Last edited: 10/31/22

    %% assumptions:
        % Nozzle extention is smooth
        % Homogeneous
        % Ideal Gas
        % Adiabatic
```

```
        % No Shocks/Discontinuities
        % Steady, Constant Flow
        % Axial Flow
        % Uniform Flow
        % Frozen Flow (chemical equilibrium)
        % Frictionless/Negligile Boundary Layer (for nominal
calculations)
        %109 %

    %% constants
    Re = 45.15; %[in] Nozzle exit Diamer = 90.3 in
    in2m  = 0.0254 ;% [m];
    Ae = pi * Re * Re * in2m *in2m;
    g_o = 9.81; %gravity m/s^2
    p_3 = 101325; %atmosphereic pressure Pa

    %% Energy Balance method
    p_2 = exit_pressure(E,k,p_1); %nominal exit pressure
    P2 = [p_2,p_2];
    P1 = [p_1,p_1];
    M_dot = [m_dot,m_dot];
    u_2 = exit_v(k,R,T_1,P2(1),P1(1)); %exit velocity assuming no
pressure loss
    u_2r = exit_vr(k,R,T_1,P2(1),P1(1),delta_p,g_o); %exit velocity
assuming there is pressure loss
    v_exit = [u_2,u_2r]; %nominal and real exit velocity

    %% Direct Method
%    p1_new = p_1 - delta_p;
%    p_2 = exit_pressure(E,k,p_1); %nominal exit pressure
%    p_2r = exit_pressure(E,k,p1_new); %exit pressure with friction
%    P2 = [p_2,p_2r];
%    P1 = [p_1, p1_new];
%    u_2 = exit_v(k,R,T_1,P2(1),P1(1)); %exit velocity assuming no
pressure loss
%    u_2r = exit_v(k,R,T_1,P2(2),P1(2));
%    v_exit = [u_2,u_2r]; %nominal and real exit velocity
%    m_dot = massflow(A_t,p_1,k,R,T_1);
%    m_dot_r = massflow(A_t,p1_new,k,R,T_1);
%    M_dot = [m_dot,m_dot_r];

    %% calculate thrust and Isp using Energy Balance Method
    for i = 1:length(P1)

        Thrust(i) = double(M_dot(i)*v_exit(i) + Ae*(P2(i) - p_3));
        ThrustVac(i) = double(M_dot(i)*v_exit(i) + Ae*(P2(i)));
        Isp(i) = double(Thrust(i)/(M_dot(i)*g_o)); %specific impulse
        IspVac(i) = double(ThrustVac(i)/(M_dot(i)*g_o));
        C_f(i) = double(Thrust(i)/(P1(i)*A_t));
        C_fVac(i) = double(ThrustVac(i)/(P1(i)*A_t));

    end
end
```

```
function PlotSL(Table1,name)

    Surface_Roughness = table2array(Table1(:,2)); % [micrometre]
    Thrust_Augmented1 =  table2array(Table1(:,5)); % [N]
    Thrust_Nominal1 = table2array(Table1(:,4)); % [N]
    Isp_Augmented1 = table2array(Table1(:,7)); % s
    Isp_Nominal1 = table2array(Table1(:,6)); % s

        figure
        hold on;
        grid on;

        yyaxis left
        plot(Surface_Roughness,Thrust_Nominal1,'r--','MarkerSize',12);
        plot(Surface_Roughness,Thrust_Augmented1,'r*-','MarkerSize',8);
        ylabel('Thrust (N)');


text(Surface_Roughness(1,1),Thrust_Augmented1(1,1),'\leftarrowUAM');

text(Surface_Roughness(2,1),Thrust_Augmented1(2,1),'\leftarrowCS');

text(Surface_Roughness(3,1),Thrust_Augmented1(3,1),'\leftarrowL-PBF and
BinderJet');
        text(39,Thrust_Augmented1(5,1),'\leftarrowEB-PBF and LP-DED');

text(Surface_Roughness(7,1),Thrust_Augmented1(7,1),'\leftarrowLW-DED');
        t =
text(Surface_Roughness(8,1),Thrust_Augmented1(8,1),'\leftarrowAW-DED
and EBW-DED');
        s = t.Rotation;
        t.Rotation = 45;
        t1 =
text(Surface_Roughness(10,1),Thrust_Augmented1(10,1),'\leftarrowAFS-
D');
        s1 = t1.Rotation;
        t1.Rotation = 45;
        xticks([7 15 40 60 200 250]);

        yyaxis right
        plot(Surface_Roughness,Isp_Nominal1,'b--','MarkerSize',12);
        plot(Surface_Roughness,Isp_Augmented1,'bo-','MarkerSize',8);
        ylabel('Isp (s)')
        xlim([0,300])
        ylim([360,372])

        ax = gca;
        ax.YAxis(1).Color = 'r';
        ax.YAxis(2).Color = 'b';

        legend('Nominal Thrust','Augmented Thrust','Nominal
Isp','Augmented Isp','Location','east');
        xlabel('Surface Roughness Ra (micrometer)');
        title(['Method ',num2str(name),':'])
        subtitle('Thrust and Isp vs Ra (Sea Level)')
    hold off
end
```

```
function PlotVac(Table1,name)

    Surface_Roughness = table2array(Table1(:,2)); % [micrometre]
    Thrust_Augmented2 =  table2array(Table1(:,9)); % [N]
    Thrust_Nominal2 = table2array(Table1(:,8)); % [N]
    Isp_Augmented2 = table2array(Table1(:,11)); % s
    Isp_Nominal2 = table2array(Table1(:,10)); % s

        figure
        hold on;
        grid on;

        yyaxis left
        plot(Surface_Roughness,Thrust_Nominal2,'r--','MarkerSize',12);
        plot(Surface_Roughness,Thrust_Augmented2,'r*-','MarkerSize',8);
        ylabel('Thrust (N)');


text(Surface_Roughness(1,1),Thrust_Augmented2(1,1),'\leftarrowUAM');

text(Surface_Roughness(2,1),Thrust_Augmented2(2,1),'\leftarrowCS');

text(Surface_Roughness(3,1),Thrust_Augmented2(3,1),'\leftarrowL-PBF and
BinderJet');
        text(39,Thrust_Augmented2(5,1),'\leftarrowEB-PBF and LP-DED');

text(Surface_Roughness(7,1),Thrust_Augmented2(7,1),'\leftarrowLW-DED');
        t =
text(Surface_Roughness(8,1),Thrust_Augmented2(8,1),'\leftarrowAW-DED
and EBW-DED');
        s = t.Rotation;
        t.Rotation = 45;
        t1 =
text(Surface_Roughness(10,1),Thrust_Augmented2(10,1),'\leftarrowAFS-
D');
        s1 = t1.Rotation;
        t1.Rotation = 45;
        xticks([7 15 40 60 200 250]);

        yyaxis right
        plot(Surface_Roughness,Isp_Nominal2,'b--','MarkerSize',12);
        plot(Surface_Roughness,Isp_Augmented2,'bo-','MarkerSize',8);
        ylabel('Isp (s)')
        xlim([0,300])

        ax = gca;
        ax.YAxis(1).Color = 'r';
        ax.YAxis(2).Color = 'b';

        legend('Nominal Thrust','Augmented Thrust','Nominal
Isp','Augmented Isp','Location','east');
        xlabel('Surface Roughness Ra (micrometer)');
        title(['Method ',num2str(name),':'])
        subtitle('Thrust and Isp vs Ra (Vacuum)')
```

```
        hold off

end


function p_2 = exit_pressure(E,k,p_1)
%exit Pressure calculates the exit pressure of a rocket nozzle
%   Inputs (in order): expansion ratio, k, chamber pressure %Eq.3.25 in
%   Sutton;
    syms p2
        S = vpasolve(1/E == (((k+1)/2)^(1/(k-
1)))*((p2/p_1)^(1/k))*sqrt(((k+1)/(k-1))*(1 - ((p2/p_1)^((k-1)/k)))));
        p_2 = S; %p_2 is exit pressure
end


function u_2_r = exit_vr(k,R,T_1,p_2,p_1,delta_p,g_o)
%Function calculates exit velocity of the rocket nozzle including power
%loss
%   Inputs: (in order): k, R, chamber temp, exit p, chamber p
u_2_r = sqrt((-2*delta_p) + (((2*k)/(k-1))*R*T_1*(1 - ((p_2/p_1)^((k-
1)/k))))); %Exit Velocity

end


function [u_2] = exit_v(k,R,T_1,p_2,p_1)
%Function calculates exit velocity of the rocket nozzle
%   Inputs: (in order): k, R, chamber temp, exit p, chamber p
u_2 = sqrt(((2*k)/(k-1))*R*T_1*(1 - ((p_2/p_1)^((k-1)/k)))); %Exit
Velocity

end
```